5-17-2001

Measurement of Dijet Production in Neutral Current Deep Inelastic Scattering at High Q^2 and Determination of α_s

J. Breitweg
Argonne National Laboratory

S. Chekanov
Argonne National Laboratory

M. Derrick
Argonne National Laboratory

D. Krakauer
Argonne National Laboratory

S. Magill
Argonne National Laboratory

Measurement of dijet production in neutral current deep inelastic scattering at high Q^2 and determination of α_s

ZEUS Collaboration

Abstract

Dijet production has been studied in neutral current deep inelastic e^+p scattering for $470 < Q^2 < 20000$ GeV^2 with the ZEUS detector at HERA using an integrated luminosity of 38.4 pb^{-1}. Dijet differential cross sections are presented in a kinematic region where both theoretical and experimental uncertainties are small. Next-to-leading-order (NLO) QCD calculations describe the measured differential cross sections well. A QCD analysis of the measured dijet fraction as a function of Q^2 allows both a precise determination of $\alpha_s(M_Z)$ and a test of the energy-scale dependence of the strong coupling constant. A detailed analysis provides an improved estimate of the uncertainties of the NLO QCD cross sections arising from the parton distribution functions of the proton. The value of $\alpha_s(M_Z)$, as determined from the QCD fit, is $\alpha_s(M_Z) = 0.1166 \pm 0.0019\ (\text{stat.})^{+0.0024}_{-0.0033}\ (\text{exp.})^{+0.0057}_{-0.0044}\ (\text{th.})$.

The ZEUS Collaboration

J. Breitweg, S. Chekanov, M. Derrick, D. Krakauer, S. Magill, B. Musgrave, A. Pellegrino, J. Repond, R. Stanek, R. Yoshida
Argonne National Laboratory, Argonne, IL, USA [p]

M.C.K. Mattingly
Andrews University, Berrien Springs, MI, USA

P. Antonioli, G. Bari, M. Basile, L. Bellagamba, D. Boscherini[1], A. Bruni, G. Bruni, G. Cara Romeo, L. Cifarelli[2], F. Cindolo, A. Contin, M. Corradi, S. De Pasquale, P. Giusti, G. Iacobucci, G. Levi, A. Margotti, T. Massam, R. Nania, F. Palmonari, A. Pesci, G. Sartorelli, A. Zichichi
University and INFN Bologna, Bologna, Italy [f]

G. Aghuzumtsyan, C. Amelung[3], I. Brock, K. Coböken[4], S. Goers, H. Hartmann, K. Heinloth[5], E. Hilger, P. Irrgang, H.-P. Jakob, A. Kappes[6], U.F. Katz, R. Kerger, O. Kind, E. Paul, J. Rautenberg, H. Schnurbusch, A. Stifutkin, J. Tandler, K.C. Voss, A. Weber, H. Wieber
Physikalisches Institut der Universität Bonn, Bonn, Germany [c]

D.S. Bailey, O. Barret, N.H. Brook[7], J.E. Cole, B. Foster[1], G.P. Heath, H.F. Heath, S. Robins, E. Rodrigues[8], J. Scott, R.J. Tapper
H.H. Wills Physics Laboratory, University of Bristol, Bristol, U.K. [o]

M. Capua, A. Mastroberardino, M. Schioppa, G. Susinno
Calabria University, Physics Dept.and INFN, Cosenza, Italy [f]

H.Y. Jeoung, J.Y. Kim, J.H. Lee, I.T. Lim, K.J. Ma, M.Y. Pac[9]
Chonnam National University, Kwangju, Korea [h]

A. Caldwell, W. Liu, X. Liu, B. Mellado, S. Paganis, S. Sampson, W.B. Schmidke, F. Sciulli
Columbia University, Nevis Labs., Irvington on Hudson, N.Y., USA [q]

J. Chwastowski, A. Eskreys, J. Figiel, K. Klimek, K. Olkiewicz, M.B. Przybycień[10], P. Stopa, L. Zawiejski
Inst. of Nuclear Physics, Cracow, Poland [j]

B. Bednarek, K. Jeleń, D. Kisielewska, A.M. Kowal, T. Kowalski, M. Przybycień, E. Rulikowska-Zarębska, L. Suszycki, D. Szuba
Faculty of Physics and Nuclear Techniques, Academy of Mining and Metallurgy, Cracow, Poland [j]

A. Kotański
Jagellonian Univ., Dept. of Physics, Cracow, Poland

L.A.T. Bauerdick, U. Behrens, J.K. Bienlein, K. Borras, V. Chiochia, J. Crittenden[11], D. Dannheim, K. Desler, G. Drews, A. Fox-Murphy, U. Fricke, F. Goebel, P. Göttlicher, R. Graciani, T. Haas, W. Hain, G.F. Hartner, K. Hebbel, S. Hillert, W. Koch[12]†, U. Kötz, H. Kowalski, H. Labes, B. Löhr, R. Mankel, J. Martens, M. Martínez, M. Milite, M. Moritz, D. Notz, M.C. Petrucci, A. Polini, M. Rohde[5], A.A. Savin, U. Schneekloth, F. Selonke, S. Stonjek, G. Wolf, U. Wollmer, C. Youngman, W. Zeuner
Deutsches Elektronen-Synchrotron DESY, Hamburg, Germany

C. Coldewey, A. Lopez-Duran Viani, A. Meyer, S. Schlenstedt, P.B. Straub
DESY Zeuthen, Zeuthen, Germany

G. Barbagli, E. Gallo, A. Parenti, P. G. Pelfer
University and INFN, Florence, Italy [f]

A. Bamberger, A. Benen, N. Coppola, S. Eisenhardt[13], P. Markun, H. Raach, S. Wölfle
Fakultät für Physik der Universität Freiburg i.Br., Freiburg i.Br., Germany [c]

M. Bell, P.J. Bussey, A.T. Doyle, C. Glasman, S.W. Lee, A. Lupi, N. Macdonald, G.J. McCance, D.H. Saxon, L.E. Sinclair, I.O. Skillicorn, R. Waugh
Dept. of Physics and Astronomy, University of Glasgow, Glasgow, U.K. [o]

B. Bodmann, N. Gendner, U. Holm, H. Salehi, K. Wick, A. Yildirim, A. Ziegler
Hamburg University, I. Institute of Exp. Physics, Hamburg, Germany [c]

T. Carli, A. Garfagnini, A. Geiser, I. Gialas[14], D. Kçira[15], E. Lohrmann
Hamburg University, II. Institute of Exp. Physics, Hamburg, Germany [c]

R. Gonçalo[8], K.R. Long, D.B. Miller, A.D. Tapper, R. Walker
Imperial College London, High Energy Nuclear Physics Group, London, U.K. [o]

P. Cloth, D. Filges
Forschungszentrum Jülich, Institut für Kernphysik, Jülich, Germany

T. Ishii, M. Kuze, K. Nagano, K. Tokushuku[16], S. Yamada, Y. Yamazaki
Institute of Particle and Nuclear Studies, KEK, Tsukuba, Japan [g]

A.N. Barakbaev, E.G. Boos, N.S. Pokrovskiy, B.O. Zhautykov
Institute of Physics and Technology of Ministry of Education and Science of Kazakhstan, Almaty, Kazakhstan

S.H. Ahn, S.B. Lee, S.K. Park
Korea University, Seoul, Korea [h]

H. Lim[17], D. Son
Kyungpook National University, Taegu, Korea [h]

F. Barreiro, G. García, O. González, L. Labarga, J. del Peso, I. Redondo[18], J. Terrón, M. Vázquez
Univer. Autónoma Madrid, Depto de Física Teórica, Madrid, Spain [n]

M. Barbi, F. Corriveau, S. Padhi, D.G. Stairs, M. Wing
McGill University, Dept. of Physics, Montréal, Québec, Canada [a], [b]

T. Tsurugai
Meiji Gakuin University, Faculty of General Education, Yokohama, Japan

A. Antonov, V. Bashkirov[19], P. Danilov, B.A. Dolgoshein, D. Gladkov, V. Sosnovtsev, S. Suchkov
Moscow Engineering Physics Institute, Moscow, Russia [l]

R.K. Dementiev, P.F. Ermolov, Yu.A. Golubkov, I.I. Katkov, L.A. Khein, N.A. Korotkova, I.A. Korzhavina, V.A. Kuzmin, O.Yu. Lukina, A.S. Proskuryakov, L.M. Shcheglova, A.N. Solomin, N.N. Vlasov, S.A. Zotkin
Moscow State University, Institute of Nuclear Physics, Moscow, Russia [m]

C. Bokel, M. Botje, J. Engelen, S. Grijpink, E. Koffeman, P. Kooijman, S. Schagen, A. van Sighem, E. Tassi, H. Tiecke, N. Tuning, J.J. Velthuis, J. Vossebeld, L. Wiggers, E. de Wolf
NIKHEF and University of Amsterdam, Amsterdam, Netherlands [i]

N. Brümmer, B. Bylsma, L.S. Durkin, J. Gilmore, C.M. Ginsburg, C.L. Kim, T.Y. Ling
Ohio State University, Physics Department, Columbus, Ohio, USA [p]

S. Boogert, A.M. Cooper-Sarkar, R.C.E. Devenish, J. Große-Knetter[20], T. Matsushita, O. Ruske, M.R. Sutton, R. Walczak
Department of Physics, University of Oxford, Oxford U.K. [o]

A. Bertolin, R. Brugnera, R. Carlin, F. Dal Corso, S. Dusini, S. Limentani, A. Longhin, M. Posocco, L. Stanco, M. Turcato
Dipartimento di Fisica dell' Università and INFN, Padova, Italy [f]

L. Adamczyk[21], L. Iannotti[21], B.Y. Oh, J.R. Okrasiński, P.R.B. Saull[21], W.S. Toothacker[12]†, J.J. Whitmore
Pennsylvania State University, Dept. of Physics, University Park, PA, USA [q]

Y. Iga
Polytechnic University, Sagamihara, Japan [g]

G. D'Agostini, G. Marini, A. Nigro
Dipartimento di Fisica, Univ. 'La Sapienza' and INFN, Rome, Italy [f]

C. Cormack, J.C. Hart, N.A. McCubbin, T.P. Shah
Rutherford Appleton Laboratory, Chilton, Didcot, Oxon, U.K. [o]

D. Epperson, C. Heusch, H.F.-W. Sadrozinski, A. Seiden, R. Wichmann, D.C. Williams
University of California, Santa Cruz, CA, USA [p]

I.H. Park
Seoul National University, Seoul, Korea

N. Pavel
Fachbereich Physik der Universität-Gesamthochschule Siegen, Germany [c]

H. Abramowicz[22], S. Dagan, A. Gabareen, S. Kananov, A. Kreisel, A. Levy
Raymond and Beverly Sackler Faculty of Exact Sciences, School of Physics, Tel-Aviv University, Tel-Aviv, Israel [e]

T. Abe, T. Fusayasu, T. Kohno, K. Umemori, T. Yamashita
Department of Physics, University of Tokyo, Tokyo, Japan [g]

R. Hamatsu, T. Hirose, M. Inuzuka, S. Kitamura[23], K. Matsuzawa, T. Nishimura
Tokyo Metropolitan University, Dept. of Physics, Tokyo, Japan [g]

M. Arneodo[24], N. Cartiglia, R. Cirio, M. Costa, M.I. Ferrero, S. Maselli, V. Monaco, C. Peroni, M. Ruspa, R. Sacchi, A. Solano, A. Staiano
Università di Torino, Dipartimento di Fisica Sperimentale and INFN, Torino, Italy [f]

D.C. Bailey, C.-P. Fagerstroem, R. Galea, T. Koop, G.M. Levman, J.F. Martin, A. Mirea, A. Sabetfakhri
University of Toronto, Dept. of Physics, Toronto, Ont., Canada [a]

J.M. Butterworth, C. Gwenlan, M.E. Hayes, E.A. Heaphy, T.W. Jones, J.B. Lane, B.J. West
University College London, Physics and Astronomy Dept., London, U.K. [o]

J. Ciborowski, R. Ciesielski, G. Grzelak, R.J. Nowak, J.M. Pawlak, R. Pawlak, B. Smalska[25], T. Tymieniecka, A.K. Wróblewski, J.A. Zakrzewski, A.F. Żarnecki
Warsaw University, Institute of Experimental Physics, Warsaw, Poland [j]

M. Adamus, T. Gadaj
Institute for Nuclear Studies, Warsaw, Poland [j]

O. Deppe[26], Y. Eisenberg, L.K. Gladilin[27], D. Hochman, U. Karshon
Weizmann Institute, Department of Particle Physics, Rehovot, Israel [d]

W.F. Badgett, D. Chapin, R. Cross, C. Foudas, S. Mattingly, D.D. Reeder, W.H. Smith, A. Vaiciulis[28], T. Wildschek, M. Wodarczyk
University of Wisconsin, Dept. of Physics, Madison, WI, USA [p]

A. Deshpande, S. Dhawan, V.W. Hughes
Yale University, Department of Physics, New Haven, CT, USA [p]

S. Bhadra, C.D. Catterall, W.R. Frisken, R. Hall-Wilton, M. Khakzad, S. Menary
York University, Dept. of Physics, Toronto, Ont., Canada [a]

[1] now visiting scientist at DESY
[2] now at Univ. of Salerno and INFN Napoli, Italy
[3] now at CERN
[4] now at Sparkasse Bonn, Germany
[5] retired
[6] supported by the GIF, contract I-523-13.7/97
[7] PPARC Advanced fellow
[8] supported by the Portuguese Foundation for Science and Technology (FCT)
[9] now at Dongshin University, Naju, Korea
[10] now at Northwestern Univ., Evaston/IL, USA
[11] on leave of absence from Bonn University
[12] deceased
[13] now at University of Edinburgh, Edinburgh, U.K.
[14] visitor of Univ. of the Aegean, Greece
[15] supported by DAAD, Bonn - Kz. A/98/12712
[16] also at University of Tokyo
[17] partly supported by an ICSC-World Laboratory Björn H. Wiik Scholarship
[18] supported by the Comunidad Autonoma de Madrid
[19] now at Loma Linda University, Loma Linda, CA, USA
[20] supported by the Feodor Lynen Program of the Alexander von Humboldt foundation
[21] partly supported by Tel Aviv University
[22] an Alexander von Humboldt Fellow at University of Hamburg
[23] present address: Tokyo Metropolitan University of Health Sciences, Tokyo 116-8551, Japan
[24] now also at Università del Piemonte Orientale, I-28100 Novara, Italy
[25] supported by the Polish State Committee for Scientific Research, grant no. 2P03B 002 19
[26] now at EVOTEC BioSystems AG, Hamburg, Germany
[27] on leave from MSU, partly supported by University of Wisconsin via the U.S.-Israel BSF
[28] now at University of Rochester, Rochester, NY, USA

[a] supported by the Natural Sciences and Engineering Research Council of Canada (NSERC)

[b] supported by the FCAR of Québec, Canada

[c] supported by the German Federal Ministry for Education and Science, Research and Technology (BMBF), under contract numbers 057BN19P, 057FR19P, 057HH19P, 057HH29P, 057SI75I

[d] supported by the MINERVA Gesellschaft für Forschung GmbH, the Israel Science Foundation, the U.S.-Israel Binational Science Foundation, the Israel Ministry of Science and the Benozyio Center for High Energy Physics

[e] supported by the German-Israeli Foundation, the Israel Science Foundation, the U.S.-Israel Binational Science Foundation, and by the Israel Ministry of Science

[f] supported by the Italian National Institute for Nuclear Physics (INFN)

[g] supported by the Japanese Ministry of Education, Science and Culture (the Monbusho) and its grants for Scientific Research

[h] supported by the Korean Ministry of Education and Korea Science and Engineering Foundation

[i] supported by the Netherlands Foundation for Research on Matter (FOM)

[j] supported by the Polish State Committee for Scientific Research, grant No. 111/E-356/SPUB-M/DESY/P-03/DZ 3001/2000, 620/E-77/SPUB-M/DESY/P-03/DZ 247/2000, and by the German Federal Ministry of Education and Science, Research and Technology (BMBF)

[l] partially supported by the German Federal Ministry for Education and Science, Research and Technology (BMBF)

[m] supported by the Fund for Fundamental Research of Russian Ministry for Science and Education and by the German Federal Ministry for Education and Science, Research and Technology (BMBF)

[n] supported by the Spanish Ministry of Education and Science through funds provided by CICYT

[o] supported by the Particle Physics and Astronomy Research Council

[p] supported by the US Department of Energy

[q] supported by the US National Science Foundation

1 Introduction

Dijet production in neutral current (NC) e^+p deep inelastic scattering (DIS) provides a rich testing ground of the theory of the strong interactions of quarks and gluons, namely quantum chromodynamics (QCD). At leading order (LO) in the strong coupling constant, α_s, 2+1 jet production[1] in NC DIS proceeds via the QCD-Compton ($V^*q \to qg$ with $V = \gamma$, Z^0) and boson-gluon fusion ($V^*g \to q\overline{q}$) processes. Thus, the differential cross section for dijet production is directly sensitive to α_s, which is the fundamental parameter of the theory. Selecting a phase-space region where the perturbative QCD (pQCD) predictions are least affected by theoretical uncertainties provides a compelling test of QCD and permits a precise determination of the strong coupling constant.

In this paper, measurements of the differential cross sections for dijet production in NC DIS are presented and compared with next-to-leading-order (NLO) pQCD predictions after correction for hadronisation effects. The phase-space region is restricted to high values of the virtuality, Q^2, of the exchanged boson, $470 < Q^2 < 20000$ GeV^2. In this region, the experimental uncertainties on the reconstruction of both the positron and the hadronic final state are smaller than at lower Q^2. In addition, the theoretical uncertainties due to the modelling of the hadronic final state, to the parton distribution functions (PDFs) of the proton and to the higher-order contributions are minimised. The comparison of the differential cross sections with the theoretical predictions of the underlying hard processes provides a test of the NLO QCD description of dijet production. The analysis takes fully into account the correlation between the value of $\alpha_s(M_Z)$ used in the determination of the proton PDFs and that in the calculation of the partonic cross sections. Furthermore, a detailed study of the theoretical uncertainties has been carried out which includes the statistical and correlated systematic uncertainties from each data set used in the determination of the proton PDFs. The QCD analysis yields a precise determination of $\alpha_s(M_Z)$ and its energy-scale dependence. The twelve-fold increase in integrated luminosity, in combination with the improved experimental and theoretical methods used here, produces a significantly more accurate determination of $\alpha_s(M_Z)$ with respect to the previous ZEUS measurement [1].

2 Theoretical framework

2.1 Kinematics

For a given e^+p centre-of-mass energy, $\sqrt{s}$, the cross section for NC DIS, $e^+p \to e^+ + \mathrm{X}$, depends on two independent kinematic variables, which are chosen to be Q^2 and the

[1] Hereafter we denote the proton remnant by "+1".

Bjorken scaling variable, x_{Bj}, where $Q^2 = -q^2$ and $x_{Bj} = Q^2/(2P \cdot q)$, and P (q) is the four-momentum of the incoming proton (exchanged virtual boson, V^*).

For dijet production in NC DIS at LO, three additional variables, ξ, z_p and Φ, are needed in order to describe the kinematics of the two outgoing massless partons which form the two jets. The fraction ξ of the proton four-momentum carried by the incoming parton is defined by $\xi = x_{Bj} \cdot (1 + M_{12}^2/Q^2)$, where M_{12} is the invariant mass of the two final-state partons. The variable z_p is defined for each outgoing parton i ($i = 1, 2$) with four-momentum p_i by

$$z_{p,i} = \frac{P \cdot p_i}{P \cdot q} = \frac{1}{2} \cdot (1 - \cos\theta_i^*) \simeq \frac{E_L^{\text{jet},i}(1 - \cos\theta_L^{\text{jet},i})}{\sum_{k=1,2} E_L^{\text{jet},k}(1 - \cos\theta_L^{\text{jet},k})},$$

where θ_i^* is the parton scattering angle in the incoming parton-V^* centre-of-mass system and $z_{p,1} + z_{p,2} = 1$. Experimentally, z_p can be determined from the energy, E_L^{jet}, and polar angle, θ_L^{jet}, of each of the two reconstructed jets in the laboratory frame. The angle Φ is the azimuthal angle between the parton and lepton scattering planes in the V^*-parton centre-of-mass system.

2.2 Cross-section calculation

According to the QCD-improved parton model, as quantitatively expressed by the factorisation theorem of QCD [2] and perturbation theory, a NC DIS differential cross section[2], $d\sigma$, can be written as

$$d\sigma = \sum_{a=q,\overline{q},g} \int dx f_a(x, \mu_F^2; \alpha_s; \{\zeta\}) \cdot d\hat{\sigma}_a(xP, \alpha_s(\mu_R), \mu_R^2, \mu_F^2) \ \cdot (1 + \delta_{\text{had}}), \qquad (1)$$

which can be interpreted as follows. The cross section has the form of a convolution of the partonic hard cross sections, $d\hat{\sigma}_a$, with the PDFs, $f_a(x, \mu_F^2)$, of the colliding proton, with respect to the fraction x of the proton four-momentum carried by the incoming parton. The partonic cross sections describe the short-distance structure of the interaction and are calculable as power-series expansions in the strong coupling constant, which depends on the renormalisation scale, μ_R. The PDFs contain the description of the long-distance structure of the incoming proton. Their evolution with the factorisation scale, μ_F, at which they are probed follows the DGLAP equations [3]. In Eq. (1), the dependence of the PDFs on the value of the strong coupling constant assumed in the DGLAP equations and on the parameters (collectively indicated by $\{\zeta\}$) needed to model the x dependence

[2] The same symbol, $d\sigma$, is used for both the DIS inclusive, $d\sigma_{\text{tot}}$, and the dijet, $d\sigma_{2+1}$, differential cross sections. The same symbols with the superscript NLO indicate only the perturbative component (the first term on the right-hand side of Eq. (1)).

of the PDFs is explicitly indicated. In this analysis, the implicit $\alpha_s(M_Z)$ dependence of the PDFs in the calculation of the NLO differential cross sections has been taken into account. The non-perturbative contribution, $\delta_{\rm had}$, to the inclusive DIS cross section, $\sigma_{\rm tot}$, can be safely neglected in the high-Q^2 region studied here. For the differential dijet cross sections, $\delta_{\rm had}$ was estimated using Monte Carlo (MC) models for the parton cascade and fragmentation (see Section 4).

In the past few years there has been considerable theoretical progress on the development of general (i.e. process- and observable-independent) algorithms that allow a complete analytical cancellation of the soft and collinear singularities encountered in the calculation of NLO jet cross sections [4, 5]; flexible programs that compute arbitrary infrared- and collinear-safe DIS observables in NLO QCD are now available [5–8].

3 Experimental setup

The data sample was collected with the ZEUS detector [9] during the 1996-1997 data-taking period at HERA and corresponds to an integrated luminosity of 38.4 ± 0.6 pb^{-1}. During this period HERA operated with protons of energy $E_p = 820$ GeV and positrons of energy $E_e = 27.5$ GeV.

The compensating uranium-scintillator calorimeter (CAL) [10] covers 99.7% of the total solid angle. It is divided into three parts with respect to the polar angle[3], θ, as viewed from the nominal interaction point: forward (FCAL, $2.6^\circ < \theta < 36.7^\circ$), barrel (BCAL, $36.7^\circ < \theta < 129.1^\circ$), and rear (RCAL, $129.1^\circ < \theta < 176.2^\circ$). Each section is sub-divided into towers which subtend solid angles between 0.006 and 0.04 steradian. Each tower is longitudinally segmented into an electromagnetic and one (RCAL) or two (FCAL, BCAL) hadronic sections. The electromagnetic section of each tower is further sub-divided transversely into two (RCAL) or four (BCAL, FCAL) cells. Under test-beam conditions, the calorimeter single-particle relative resolutions were $18\%/\sqrt{E\,(\mathrm{GeV})}$ for electrons and $35\%/\sqrt{E\,(\mathrm{GeV})}$ for hadrons.

Tracking information is provided by the central tracking detector (CTD) [11] operating in a 1.43 T solenoidal magnetic field. The interaction vertex is measured with a typical resolution along (transverse to) the beam direction of 0.4 (0.1) cm. The CTD is used to reconstruct the momenta of tracks in the polar angle region $15^\circ < \theta < 164^\circ$.

[3] The ZEUS coordinate system is a right-handed Cartesian system, with the Z axis pointing in the proton beam direction, referred to as the "forward direction", and the X axis pointing left towards the centre of HERA. The coordinate origin is at the nominal interaction point. The pseudorapidity is defined as $\eta = -\ln\left(\tan\frac{\theta}{2}\right)$, where the polar angle, θ, is measured with respect to the proton beam direction.

The transverse momentum, p_t, resolution for full-length tracks can be parameterised as $\sigma(p_t)/p_t = 0.0058\ p_t \oplus 0.0065 \oplus 0.0014/p_t$, with p_t in GeV.

The luminosity is measured using the Bethe-Heitler reaction $e^+p \to e^+\gamma p$ [12]. The resulting small-angle energetic photons are measured by the luminosity monitor, a lead-scintillator calorimeter placed in the HERA tunnel at $Z = -107$ m.

4 Monte Carlo models

NC DIS events including radiative effects were simulated using the HERACLES 4.5.2 [13] MC program with the DJANGO6 2.4 [14] interface to the hadronisation programs. HERACLES includes corrections for initial- and final-state radiation, vertex and propagator terms, and two-boson exchange. The QCD cascade is simulated using the colour-dipole model [15] including the LO QCD diagrams as implemented[4] in ARIADNE 4.08 [17] and, as a systematic check of the final results, with the MEPS model of LEPTO 6.5 [18]. Both MC programs use the Lund string model [19] of JETSET 7.4 [20] for the hadronisation. To estimate the uncertainty caused by the modelling of hadronisation, events were also generated with the HERWIG 5.9 [21] program, in which the fragmentation is simulated according to a cluster model [22].

The ZEUS detector response was simulated with a program based on GEANT 3.13 [23]. The generated events were passed through the simulated detector, subjected to the same trigger requirements as the data, and processed by the same reconstruction and offline programs.

The simulations based on ARIADNE and LEPTO give a very good description of the shape and magnitude of the measured distributions of the inclusive event sample as a function of x_{Bj} and Q^2. The shape of most of the measured distributions of the dijet sample is also adequately described by these two programs. LEPTO gives a better description of the jet pseudorapidity distributions, while ARIADNE gives a better description of the shape of the dijet cross section as a function of Q^2. ARIADNE was used to calculate the acceptance corrections; both programs give very similar results.

In addition, samples of events were generated without either Z^0 exchange or electroweak radiative events, allowing the measured cross sections to be corrected for these effects, which at present are not included in the NLO QCD programs described below.

[4] A modified treatment of parton radiation at high Q^2 [16] was included.

5 NLO QCD calculations

The NLO QCD calculations used in the analysis are based on the program DISENT [5]. The calculations make use of a generalised version [5] of the subtraction method [24] and are performed in the massless $\overline{\rm MS}$ renormalisation and factorisation schemes. The number of flavours was set to 5, the scales μ_R and μ_F were both set to Q, and $\alpha_s(\mu_R)$ was evaluated using the two-loop formula [25]. Various sets of proton PDFs, hereafter generically referred to as MBFIT PDFs[5], resulting from a recent analysis [26], were used. This analysis provides the covariance matrix of the fitted PDF parameters and the derivatives as a function of x and Q^2 of the PDFs with respect to these parameters. These are necessary to propagate the statistical and correlated systematic uncertainties of each data set used in the NLO DGLAP fit to the NLO QCD differential cross sections. The DISENT predictions have been cross-checked with results obtained with the program DISASTER++ [7]. Agreement at the $1-2\%$ level has been found between these programs for all the observables discussed in this paper.

The NLO pQCD predictions to be compared with the data were corrected by a bin-by-bin procedure for hadronisation effects according to $d\sigma_{2+1} = d\sigma_{2+1}^{NLO} \cdot C_{\rm had}^{-1}$. The hadronisation correction factor, $C_{\rm had}$ ($\equiv (1+\delta_{\rm had})^{-1}$), was defined as the ratio of the dijet cross sections before and after the hadronisation process, $C_{\rm had} = d\sigma_{2+1}^{MC,\rm partons}/d\sigma_{2+1}^{MC,\rm hadrons}$. The value of $C_{\rm had}$ was taken as the mean of the ratios obtained using the ARIADNE and HERWIG programs, for which the predictions agree typically within 5%. The hadronisation correction was below 10% for most of the phase space. These programs only include the LO matrix elements for the partonic cross sections and higher-order contributions are simulated using various approximations to the parton cascade. This procedure for applying hadronisation corrections to the NLO QCD predictions was verified by checking that the shapes of the differential dijet cross sections at the parton level are reproduced by the NLO QCD calculations at the 10% level.

6 Event selection and jet search

6.1 The NC DIS data sample

High-Q^2 NC DIS events were selected according to criteria similar to those described in a recent ZEUS publication [27]. The events are characterised by a high-energy isolated positron in the detector, making them easy to distinguish from quasi-real photoproduction ($Q^2 \sim 0$) and beam-gas interaction backgrounds.

[5] The MBFIT1M set of proton PDFs assumes $\alpha_s(M_Z) = 0.118$.

In addition to the energy and polar angle of the positron[6], the variables δ, net transverse momentum, P_T, and total transverse energy, E_T, were used for event selection, where $\delta = E - P_Z$, E is the total energy as measured in the CAL and $\boldsymbol{P} = \sum_i E_i \boldsymbol{r_i}$. The sum runs over all calorimeter energy deposits E_i, and $\boldsymbol{r_i}$ is a unit vector along the line joining the reconstructed vertex and the geometric centre of cell i. The following criteria were applied offline:

- to ensure that event quantities can be accurately determined, a reconstructed vertex with $-50 < Z < 50$ cm was required;

- to suppress photoproduction events, in which the scattered positron escapes through the beam hole in the RCAL, δ was required to be greater than 38 GeV. For perfect detector resolution, δ is twice the positron beam energy (55 GeV) for fully contained DIS events, while, for photoproduction events, δ peaks at much lower values. This cut also rejected events with hard initial-state QED radiation. The additional requirement $\delta < 65$ GeV removed cosmic ray background;

- positrons were identified based on calorimeter cluster quantities and tracking:

  - to ensure high purity, the positron was required to have an energy of at least 10 GeV;

  - to reduce background, isolated positrons were selected by requiring no more than 5 GeV in calorimeter cells not associated with the scattered positron in an $\eta - \phi$ cone of radius 0.8 centred on the positron direction;

  - each positron with $\theta_e > 17.2^\circ$ was required to match to a charged track of at least 5 GeV momentum. For positrons beyond the tracking acceptance ($\theta_e < 17.2^\circ$), the tracking requirement in the positron selection was replaced by a cut on the transverse momentum of the positron $p_T^e > 30$ GeV and by the requirement $\delta > 44$ GeV;

  - a fiducial volume cut was applied to the positron position which excludes the upper part of the central RCAL area (20×80 cm^2) occluded by the cryogenic supply for the solenoid magnet. The transition regions between FCAL and BCAL, and BCAL and RCAL, corresponding to polar angles of $35.6^\circ < \theta < 37.3^\circ$ and $128.2^\circ < \theta < 140.2^\circ$, respectively, were also excluded;

- to reduce further the background from photoproduction, the variable $y = Q^2/(x_{Bj}s)$, estimated from the positron energy and angle, y_e, was required to satisfy $y_e < 0.95$;

[6] The positron polar angle, θ_e, was determined from the associated track if the positron cluster was within the CTD acceptance, and otherwise from the position of the cluster and the reconstructed vertex.

- the net transverse momentum, P_T , is expected to be close to zero and was measured with an error approximately proportional to $\sqrt{E_T(\mathrm{GeV})}$. To remove cosmic rays and beam-related background, $P_T(\mathrm{GeV})$ was required to be less than $4\sqrt{E_T\,(\,\mathrm{GeV})}$.

The kinematic variables Q^2, x_{Bj} and y were determined using the double angle (DA) reconstruction method [28] and are referred to as $Q^2_{\mathrm{DA}}, x_{\mathrm{DA}}$ and y_{DA}, respectively. The DA method is insensitive to errors in the absolute energy scale of the calorimeter and MC studies [27] have shown it to be superior to other methods in the high-Q^2 region considered here.

6.2 Jet search and reconstruction

The longitudinally invariant k_T-cluster algorithm [29] was used in the inclusive mode to reconstruct jets in the hadronic final state both in data and in MC simulated events. At the detector level, the algorithm was applied to the energy deposits in the CAL cells after excluding those associated with the scattered positron candidate. The jet search was also applied to the generated hadrons and to the partons in the MC samples, as well as to the partons of the NLO QCD programs. The jet search was performed in the Breit frame [30], in which the exchanged virtual boson is purely space-like with three-momentum $\boldsymbol{q} = (0, 0, -Q)$. In this frame, the selection of the jets in terms of transverse energy with respect to the direction of the virtual boson allows a natural suppression of the contribution due to single-jet events and strongly reduces the contamination from the proton remnant. The boost was performed using the four-momenta of the incoming and scattered positrons. The scattered positron four-momentum was calculated using the polar and azimuthal angles of the positron track[7] and the DA positron energy, defined as $E'_{e,\mathrm{DA}} = Q^2_{\mathrm{DA}}/(2E_e(1+\cos\theta_e))$.

The jet algorithm uses quantities defined in the Breit frame and with respect to the direction of the incoming proton: the transverse energy, $E^i_{T,B}$, the pseudorapidity, η^i_B, and the azimuthal angle, ϕ^i_B, of the object i. The jet variables were defined according to the Snowmass convention [31]:

$$E^{\mathrm{jet}}_{T,B} = \sum_i E^i_{T,B}\ ,\ \eta^{\mathrm{jet}}_B = \frac{\sum_i E^i_{T,B}\ \eta^i_B}{E^{\mathrm{jet}}_{T,B}}\ ,\ \phi^{\mathrm{jet}}_B = \frac{\sum_i E^i_{T,B}\ \phi^i_B}{E^{\mathrm{jet}}_{T,B}}.$$

The comparison of the reconstructed jet variables between jets of hadrons and jets of CAL cells in MC generated events showed no significant systematic shift in the angular

[7] For events with $\theta_e < 17.2°$, the polar and azimuthal angles were calculated from the position of the positron calorimeter cluster and the reconstructed vertex position.

variables $\eta_B^{\rm jet}$ and $\phi_B^{\rm jet}$. However, the jet transverse energy as measured by the CAL underestimated that of the jet of hadrons by an average of $\approx 15\%$. This effect is due mainly to energy losses in the inactive material in front of the CAL and was corrected [32,33] using the samples of MC generated events.

6.3 Selected kinematic region

The differential cross sections and dijet fraction presented in Section 7 are quoted for the DIS kinematic region defined by $470 < Q^2 < 20000$ GeV^2 and $0 < y < 1$, and for the jet selection criteria $E_{T,B}^{{\rm jet},M} > 8$ GeV, $E_{T,B}^{{\rm jet},m} > 5$ GeV and $-1 < \eta_{Lab}^{\rm jet} < 2$, where $E_{T,B}^{{\rm jet},M}$ ($E_{T,B}^{{\rm jet},m}$) is the transverse energy of the jet in the Breit frame with the highest (second highest) transverse energy in the event. Only events with exactly two jets passing the above selection cuts were used to compute the cross sections. The final sample contains 1637 dijet events. The restriction to a high-Q^2 region was chosen to avoid the large renormalisation-scale dependence of the NLO QCD dijet cross sections at lower Q^2 ($20-50\%$ in the region $10 < Q^2 < 100$ GeV^2) [33], to reduce the uncertainty due to the proton PDFs (in particular the gluon density), and to improve the reconstruction of the boost to the Breit frame. The asymmetric cuts on the $E_{T,B}^{\rm jet}$ of the jets avoided infrared sensitive regions where the behaviour of the cross section as predicted by the NLO QCD programs is unphysical [34].

7 Results

7.1 Dijet differential cross sections

The cross sections measured in the kinematic region defined in the previous section were corrected for detector effects, QED radiative effects and Z^0-exchange processes. In the presented dijet cross sections, the two jets were ordered according to decreasing pseudorapidity in the Breit frame ($\eta_B^{{\rm jet},1} > \eta_B^{{\rm jet},2}$). The measurements[8] of the differential dijet cross sections are presented in Figs. 1 and 2. The inclusive and dijet cross sections, as well as the dijet fraction, $R_{2+1}(Q^2) \equiv (d\sigma_{2+1}/dQ^2)/(d\sigma_{\rm tot}/dQ^2)$, are presented as a function of Q^2 in Fig. 3.

In Figs. 1 to 3, the measured differential dijet cross sections and dijet fraction are compared to DISENT NLO QCD predictions, corrected for hadronisation effects. The hadronisation

[8] Tables of the results and their associated uncertainties are available in electronic form from the ZEUS WWW site at http://www-zeus.desy.de/zeus_papers/zeus_papers.html. They can also be obtained by contacting the authors.

correction, $C_{\rm had}$, as well as its uncertainty, and the NLO QCD cross sections without hadronisation corrections are shown in Figs. 1 to 3. The QCD predictions, which assume $\alpha_s(M_Z) = 0.118$, provide a good overall description of both the shape and the magnitude of the measured cross sections. The only case where the agreement between data and NLO QCD is not good is the cross section as a function of the pseudorapidity of the most backward jet in the Breit frame (see Fig. 2d), where the data lie above the theoretical predictions in the region $\eta_B^{\rm jet,2} > 0.5$. However, hadronisation effects are particularly large for this variable and vary more rapidly than for other variables. The impact of such a discrepancy in the determination of $\alpha_s(M_Z)$ is minor since the contribution to the total dijet cross section from the region $\eta_B^{\rm jet,2} > 0.5$ is small. The dijet fraction increases with increasing Q^2 due to phase-space effects. For the cross sections as a function of the jet transverse energies and Q^2, there is agreement at the $\approx 10\%$ level between data and theory over four orders of magnitude, demonstrating the validity of the description of the dynamics of dijet production by the NLO QCD hard processes.

7.2 Experimental and theoretical uncertainties

A detailed study of each of the main sources contributing to the systematic uncertainties of the measurements has been performed [33]. These sources, for which a typical value of the systematic uncertainty in the dijet cross section $d\sigma_{2+1}/dQ^2$ is indicated in parentheses, are listed below:

- uncertainties in the positron identification efficiency and in the positron energy-scale [27] (1%);
- uncertainties in the reconstruction of the boost to the Breit frame (1%);
- use of the LEPTO program instead of ARIADNE to evaluate the acceptance corrections to the observed dijet distributions (2%);
- uncertainties in the simulation of the trigger and in the cuts used to select the data (2%);
- uncertainty of $\pm 2\%$ in the absolute jet energy scale of the CAL ($\pm 3.5\%$) obtained by examining the transverse momentum balance between the scattered positron and the jets.

The last uncertainty is the dominant source of experimental systematic uncertainty and is strongly correlated between measurements at different points. It is shown as a light shaded band in Fig. 3b. In addition, there is an overall normalisation uncertainty of 1.6% from the luminosity determination, which is not included in the figures.

The NLO QCD predictions for the dijet cross sections are affected by the following:

- uncertainties in the hadronisation correction, which were estimated as half the spread between the $C_{\rm had}$ values obtained using the ARIADNE (string) and HERWIG (cluster) models (1%);

- uncertainties due to terms beyond NLO, which were estimated by varying μ_R between $Q/2$ and $2Q$, keeping μ_F fixed at Q (6%);

- uncertainty in the value of $\alpha_s(M_Z)$, which was estimated by repeating the calculations using MBFIT proton PDFs determined assuming $\alpha_s(M_Z) = 0.113$ and 0.123 [26] (6%);

- uncertainties in the proton PDFs. The uncertainty due to the statistical and correlated systematic experimental uncertainties of each data set used in the determination of the MBFIT PDFs was calculated making use of the covariance matrix provided [26]. To estimate the uncertainties on the NLO QCD differential cross sections due to the theoretical uncertainties affecting the extraction of the NLO PDFs, the calculation of all the differential cross sections was repeated using a number of different MBFIT PDFs obtained under different theoretical assumptions in the DGLAP fit [26]. This uncertainty was added in quadrature to that estimated above to give the total PDF-related uncertainty. The importance of taking the correlations among the PDF parameters into account is illustrated in Fig. 4, which shows, as a function of Q^2, the relative uncertainties arising from the PDFs on the inclusive and dijet cross sections, and the dijet fraction. The uncertainties were obtained by including or ignoring the information provided by the covariance matrix mentioned above. The small uncertainty on $R_{2+1}(Q^2)$ due to the PDFs makes this observable particularly suitable for extracting α_s (2.5% on $d\sigma_{\rm tot}/dQ^2$, 4% on $d\sigma_{2+1}/dQ^2$ and 1.5% on $R_{2+1}(Q^2)$).

The total theoretical uncertainty was obtained by adding in quadrature the individual uncertainties listed above.

7.3 Determination of α_s

The measured dijet fraction as a function of Q^2, $R_{2+1}(Q^2)$, was used to determine $\alpha_s(M_Z)$. The sensitivity of the measurements to the value of $\alpha_s(M_Z)$ is illustrated in Fig. 3b, which compares the measured $R_{2+1}(Q^2)$ with the NLO QCD calculations for three values of $\alpha_s(M_Z)$.

The procedure to determine $\alpha_s(M_Z)$ was as follows:

- NLO QCD calculations of $R_{2+1}(Q^2)$ were performed for three sets of MBFIT proton PDFs obtained assuming $\alpha_s(M_Z) = 0.113$, 0.118 and 0.123, respectively [26]. The value of $\alpha_s(M_Z)$ used in each partonic cross-section calculation was that associated with the corresponding set of PDFs;

- for each bin, i, in Q^2, the NLO QCD calculations mentioned above, corrected for hadronisation effects, were used to parameterise the α_s dependence of the dijet fraction according to the functional form:

$$R^i_{2+1}(\alpha_s(M_Z)) = A^i_1 \cdot \alpha_s(M_Z) + A^i_2 \cdot \alpha^2_s(M_Z). \quad (2)$$

  This parameterisation allows a simple description of the α_s dependence of $R_{2+1}(Q^2)$ over the entire α_s range spanned by the MBFIT PDF sets, while using only three NLO calculations of the dijet fraction;

- the value of $\alpha_s(M_Z)$ was then determined by a χ^2-fit of Eq. (2) to the measured $R_{2+1}(Q^2)$ values.

This procedure correctly handles the complete α_s-dependence of the NLO differential cross sections (the explicit dependence coming from the partonic cross sections and the implicit one coming from the PDFs) in the fit, while preserving the correlation between α_s and the PDFs. Its stability was checked with respect to variations in the PDFs and α_s, as well as to alternative parameterisations of $R_{2+1}(Q^2, \alpha_s(M_Z))$.

Taking into account only the statistical errors on the measured dijet fraction, $\alpha_s(M_Z)$ is found to be 0.1166 ± 0.0019 (stat.). The uncertainty on the value of $\alpha_s(M_Z)$ due to the experimental systematic uncertainties of the measured dijet fraction was evaluated by repeating the analysis above for each systematic check. For the ratio $R_{2+1}(Q^2)$, some of the systematic uncertainties largely cancel. The total experimental systematic uncertainty on the value of $\alpha_s(M_Z)$ is $^{+0.0024}_{-0.0033}$. The largest uncertainty is that on the jet energy scale.

The following sources of theoretical uncertainties (evaluated as described in Section 7.2) and cross-checks on the extracted value of $\alpha_s(M_Z)$ were considered [33]:

- terms beyond NLO: $\Delta\alpha_s(M_Z) = ^{+0.0055}_{-0.0042}$;

- uncertainties in the proton PDFs: $\Delta\alpha_s(M_Z) = ^{+0.0012}_{-0.0011}$;

- hadronisation effects: $\Delta\alpha_s(M_Z) = \pm 0.0005$;

- the dependence on the use of a renormalisation scale that involves the jet variables. The analysis was repeated with $\mu_R = (E^{\mathrm{jet},1}_{T,B} + E^{\mathrm{jet},2}_{T,B})$. The result is $\alpha_s(M_Z) = 0.1125 \pm 0.0018$ (stat.), which is almost equal to that obtained with $\mu_R = Q/2$. This source of uncertainty was therefore neglected;

- the fit procedure. This was cross-checked by repeating the $\alpha_s(M_Z)$ determination using the five sets of proton PDFs of the CTEQ4 "A-series" [35] and the three MRST sets, central, $\alpha_s \uparrow\uparrow$ and $\alpha_s \downarrow\downarrow$ [36]. The results are in good agreement with the central value determined above. This source of uncertainty was therefore neglected

The total theoretical uncertainty of $^{+0.0057}_{-0.0044}$ was obtained by adding in quadrature the uncorrelated uncertainties on $\alpha_s(M_Z)$ due to the first three items mentioned above.

The value of $\alpha_s(M_Z)$ as determined from the measured $R_{2+1}(Q^2)$ is therefore:

$$\alpha_s(M_Z) = 0.1166 \pm 0.0019\ (\text{stat.})^{+0.0024}_{-0.0033}\ (\text{exp.})^{+0.0057}_{-0.0044}\ (\text{th.}).$$

This result is consistent with the current PDG world average, $\alpha_s(M_Z) = 0.1181 \pm 0.0020$ [25], a review from Bethke [37], and recent determinations by the H1 Collaboration [38].

7.4 The energy scale dependence of α_s

A consistency test for the scale dependence of the renormalised strong coupling constant predicted by the renormalisation group equation was carried out by repeating the QCD fit of the dijet fraction in five Q^2 bins. The principle of the fit is the same as outlined above, with the only difference being that the α_s dependence of the dijet fraction in Eq. (2) was parameterised not in terms of $\alpha_s(M_Z)$ but in terms of $\alpha_s(\langle Q \rangle)$, where $\langle Q \rangle$ is the mean value of Q in each bin. The measured $\alpha_s(\langle Q \rangle)$ values, with their experimental and theoretical systematic uncertainties estimated as for $\alpha_s(M_Z)$, are shown in Fig. 5. The measurements are compared with the renormalisation group predictions obtained from the PDG $\alpha_s(M_Z)$ value and its associated uncertainty. The values are in good agreement with the predicted running of the strong coupling constant over a large range in Q.

8 Summary

Differential dijet cross sections have been measured in neutral current deep inelastic e^+p scattering for $470 < Q^2 < 20000$ GeV^2 with the ZEUS detector at HERA. These measurements, which use events with only two jets, were performed in a kinematic region where both theoretical and experimental uncertainties are small. Next-to-leading-order QCD calculations give a good description of the shape and magnitude of the kinematic distributions and cross sections. For the cross sections as a function of the jet transverse energies and Q^2, there is agreement at the $\approx 10\%$ level between data and theory over four orders of magnitude, demonstrating the validity of the description of the dynamics of dijet production by the NLO QCD hard processes. A QCD fit of the measured dijet fraction

as a function of Q^2 provides both a precise determination of the strong coupling constant and a test of its energy-scale dependence. A comprehensive analysis of the uncertainties of the calculations has been carried out, which takes into account the dependence of the proton PDFs on the assumed value of α_s and the statistical and correlated systematic uncertainties from each data set used in the determination of the proton PDFs. The value of $\alpha_s(M_Z)$ as determined by fitting the next-to-leading-order QCD calculations to the measured dijet fraction is

$$\alpha_s(M_Z) = 0.1166 \pm 0.0019\ (\text{stat.})^{+0.0024}_{-0.0033}\ (\text{exp.})^{+0.0057}_{-0.0044}\ (\text{th.})\ ,$$

in good agreement with the world average [25]. The value of α_s as a function of Q is in good agreement, over a wide range of Q, with the running of α_s as predicted by QCD.

Acknowledgements

We thank the DESY Directorate for their strong support and encouragement. The remarkable achievements of the HERA machine group were essential for the successful completion of this work and are greatly appreciated. We would like to thank D. Graudenz, M. Seymour and H. Spiesberger for valuable discussions and help in running their NLO programs.

References

[1] ZEUS Collaboration, M. Derrick et al., Phys. Lett. B 363 (1995) 201.

[2] See e.g. J.C. Collins, D.E. Soper and G. Sterman, in *Perturbative Quantum Chromodynamics*, edited by A.H. Mueller, World Scientific, Singapore (1989), p. 1 and references therein.

[3] V.N. Gribov and L.N. Lipatov, Sov. J. Nucl. Phys. 15 (1972) 438;
L.N. Lipatov, Sov. J. Nucl. Phys. 20 (1975) 94;
Y.L. Dokshitzer, Sov. Phys. JETP 46 (1977) 641;
G. Altarelli and G. Parisi, Nucl. Phys. B 126 (1977) 298.

[4] S.D. Ellis, Z. Kunszt and D.E. Soper, Phys. Rev. D 40 (1989) 2188 and Phys. Rev. Lett. 69 (1992) 1496;
Z. Kunszt and D.E. Soper, Phys. Rev. D 46 (1992) 192;
W.T. Giele and E.W.N. Glover, Phys. Rev. D 46 (1992) 1980;
W.T. Giele, E.W.N. Glover and D.A. Kosower, Nucl. Phys. B 403 (1993) 633;
S. Frixione, Z. Kunszt and A. Signer, Nucl. Phys. B 467 (1996) 399;
Z. Nagy and Z. Trocsanyi, Nucl. Phys. B 486 (1997) 189.

[5] S. Catani and M. H. Seymour, Nucl. Phys. B 485 (1997) 291 and Erratum B 510 (1997) 503.

[6] E. Mirkes and D. Zeppenfeld, Phys. Lett. B 380 (1996) 205;
E. Mirkes, TTP-97-39 (hep-ph/9711224).

[7] D. Graudenz, hep-ph/9710244.

[8] B. Pötter, Comp. Phys. Comm. 119 (1999) 45.

[9] ZEUS Collaboration, U. Holm (ed.), *The ZEUS Detector*, Status Report (unpublished), DESY, 1993, available on WWW: `http://www-zeus.desy.de/bluebook/bluebook.html`.

[10] M. Derrick et al., Nucl. Instr. and Meth. A 309 (1991) 77;
A. Andresen et al., Nucl. Instr. and Meth. A 309 (1991) 101;
A. Caldwell et al., Nucl. Instr. and Meth. A 321 (1992) 356;
A. Bernstein et al., Nucl. Instr. and Meth. A 336 (1993) 23.

[11] N. Harnew et al., Nucl. Instr. and Meth. A 279 (1989) 290;
B. Foster et al., Nucl. Phys. B (Proc. Suppl.) 32 (1993) 181;
B. Foster et al., Nucl. Instr. and Meth. A 338 (1994) 254.

[12] J. Andruszków et al., DESY 92-066 (1992);
ZEUS Collaboration, M. Derrick et al., Z. Phys. C 63 (1994) 391.

[13] K. Kwiatkowski, H. Spiesberger and H.-J. Möhring, Comp. Phys. Comm. 69 (1992) 155.

[14] K. Charchuła, G.A. Schuler, and H. Spiesberger, Comp. Phys. Comm. 81 (1994) 381.

[15] Y. Azimov et al., Phys. Lett. B 165 (1985) 147;
G. Gustafson, Phys. Lett. B 175 (1986) 453;
G. Gustafson and U. Petersson, Nucl. Phys. B 306 (1988) 746;
B. Andersson, G. Gustafson and L. Lönnblad, Z. Phys. C 43 (1989) 625.

[16] L. Lönnblad, in *Proc. Workshop on Monte Carlo Generators for HERA Physics, Apr. 1998*, eds. A.T. Doyle, G. Grindhammer, G. Ingelman and H. Jung, p. 47, Hamburg, Germany, DESY (1999) and hep-ph/9908368.

[17] L. Lönnblad, Comp. Phys. Comm. 71 (1992) 15; Z. Phys. C 65 (1995) 285.

[18] G. Ingelman, A. Edin and J. Rathsman, Comp. Phys. Comm. 101 (1997) 108.

[19] B. Andersson et al., Phys. Rep. 97 (1983) 31.

[20] H.-U. Bengtsson and T. Sjöstrand, Comp. Phys. Comm. 46 (1987) 43;
T. Sjöstrand, Comp. Phys. Comm. 82 (1994) 74.

[21] G. Marchesini et al., Comp. Phys. Comm. 67 (1992) 465.

[22] B.R. Webber, Nucl. Phys. B 238 (1984) 492.

[23] R. Brun et al., CERN-DD/EE/84-1 (1987).

[24] R.K. Ellis, D.A. Ross and A.E. Terrano, Nucl. Phys. B 178 (1981) 421.

[25] Particle Data Group, D.E. Groom et al., Eur. Phys. J. C 15 (2000) 1.

[26] M. Botje, Eur. Phys. J. C 14 (2000) 285.

[27] ZEUS Collaboration, J. Breitweg et al., Eur. Phys. J. C 11 (1999) 427.

[28] S. Bentvelsen, J. Engelen, and P. Kooijman, in *Proc. Workshop on Physics at HERA, Oct. 1991*, Volume 1, W. Buchmüller and G. Ingelman (eds.), DESY (1992), p. 23;
K. C. Hoeger, *ibid.*, p. 43.

[29] S. Catani et al., Nucl. Phys. B 406 (1993) 187;
S.D. Ellis and D.E. Soper, Phys. Rev. D 48 (1993) 3160.

[30] R.P. Feynman, *Photon-Hadron Interactions*, Benjamin, (1972);
K.H. Streng, T.F. Walsh and P.M. Zerwas, Z. Phys. C 2 (1979) 237.

[31] J. Huth et al., in *Proc. of the 1990 DPF Summer Study on High Energy Physics*, ed. E.L. Berger, p. 134, Snowmass, Colorado, World Scientific (1992).

[32] ZEUS Collaboration, J. Breitweg et al., Eur. Phys. J. C 8 (1999) 367.

[33] E. Tassi, Ph.D. Thesis, University of Hamburg (2001), in preparation.

[34] M. Klasen and G. Kramer, Phys. Lett. B 366 (1996) 385;
S. Frixione and G. Ridolfi, Nucl. Phys. B 507 (1997) 315;
B. Pötter, Comp. Phys. Comm. 133 (2000) 105.

[35] H.L. Lai et al., Phys. Rev. D 55 (1997) 1280.

[36] A.D. Martin et al., Eur. Phys. J. C 4 (1998) 463.

[37] S. Bethke, J. Phys. G26 (2000) R27.

[38] H1 Collaboration, C. Adloff et al., DESY 00-145 (2000) and DESY 00-181 (2000).

$z_{p,1}$ range	$d\sigma_{2+1}/dz_{p,1}$ [pb]	$\Delta_{\rm stat}$	$\Delta_{\rm syst}$	$\Delta_{\rm ES}$
0.00 – 0.05	$1.118 \cdot 10^1$	$(\pm 0.244) \cdot 10^1$	$(^{+0.203}_{-0.097}) \cdot 10^1$	$(^{+0.089}_{-0.089}) \cdot 10^1$
0.05 – 0.15	$9.777 \cdot 10^1$	$(\pm 0.555) \cdot 10^1$	$(^{+0.365}_{-0.519}) \cdot 10^1$	$(^{+0.365}_{-0.400}) \cdot 10^1$
0.15 – 0.25	$1.233 \cdot 10^2$	$(\pm 0.063) \cdot 10^2$	$(^{+0.024}_{-0.068}) \cdot 10^2$	$(^{+0.038}_{-0.033}) \cdot 10^2$
0.25 – 0.35	$8.469 \cdot 10^1$	$(\pm 0.520) \cdot 10^1$	$(^{+0.625}_{-0.482}) \cdot 10^1$	$(^{+0.207}_{-0.158}) \cdot 10^1$
0.35 – 0.45	$7.738 \cdot 10^1$	$(\pm 0.505) \cdot 10^1$	$(^{+0.425}_{-0.268}) \cdot 10^1$	$(^{+0.170}_{-0.144}) \cdot 10^1$
0.45 – 0.55	$5.473 \cdot 10^1$	$(\pm 0.438) \cdot 10^1$	$(^{+0.288}_{-0.145}) \cdot 10^1$	$(^{+0.125}_{-0.133}) \cdot 10^1$
0.55 – 0.65	$5.259 \cdot 10^1$	$(\pm 0.453) \cdot 10^1$	$(^{+0.156}_{-0.525}) \cdot 10^1$	$(^{+0.138}_{-0.148}) \cdot 10^1$
0.65 – 0.75	$3.938 \cdot 10^1$	$(\pm 0.415) \cdot 10^1$	$(^{+0.240}_{-0.451}) \cdot 10^1$	$(^{+0.167}_{-0.135}) \cdot 10^1$
0.75 – 0.85	$2.064 \cdot 10^1$	$(\pm 0.349) \cdot 10^1$	$(^{+0.076}_{-0.416}) \cdot 10^1$	$(^{+0.135}_{-0.137}) \cdot 10^1$
0.85 – 0.95	4.436	± 1.537	$^{+1.261}_{-1.232}$	$^{+0.522}_{-0.325}$

Table 1: The differential dijet cross section $d\sigma_{2+1}/dz_{p,1}$. For each bin in $z_{p,1}$, the measured cross section, the statistical uncertainty, $\Delta_{\rm stat}$, and the systematic uncertainty (not) associated with the energy scale of the jets, $\Delta_{\rm ES}$ ($\Delta_{\rm syst}$), are given. The overall normalisation uncertainty of 1.6% due to the luminosity determination is not included.

$\log_{10}(x_{Bj})$ range	$d\sigma_{2+1}/d\log_{10}(x_{Bj})$ [pb]	$\Delta_{\rm stat}$	$\Delta_{\rm syst}$	$\Delta_{\rm ES}$
-2.20 – -2.00	$2.681 \cdot 10^1$	$(\pm 0.267) \cdot 10^1$	$(^{+0.241}_{-0.093}) \cdot 10^1$	$(^{+0.072}_{-0.064}) \cdot 10^1$
-2.00 – -1.80	$4.794 \cdot 10^1$	$(\pm 0.286) \cdot 10^1$	$(^{+0.139}_{-0.118}) \cdot 10^1$	$(^{+0.114}_{-0.115}) \cdot 10^1$
-1.80 – -1.60	$5.902 \cdot 10^1$	$(\pm 0.312) \cdot 10^1$	$(^{+0.143}_{-0.472}) \cdot 10^1$	$(^{+0.162}_{-0.166}) \cdot 10^1$
-1.60 – -1.40	$5.821 \cdot 10^1$	$(\pm 0.319) \cdot 10^1$	$(^{+0.110}_{-0.497}) \cdot 10^1$	$(^{+0.175}_{-0.180}) \cdot 10^1$
-1.40 – -1.20	$4.105 \cdot 10^1$	$(\pm 0.263) \cdot 10^1$	$(^{+0.341}_{-0.141}) \cdot 10^1$	$(^{+0.146}_{-0.138}) \cdot 10^1$
-1.20 – -1.00	$2.750 \cdot 10^1$	$(\pm 0.203) \cdot 10^1$	$(^{+0.112}_{-0.181}) \cdot 10^1$	$(^{+0.095}_{-0.070}) \cdot 10^1$
-1.00 – -0.80	$1.195 \cdot 10^1$	$(\pm 0.131) \cdot 10^1$	$(^{+0.155}_{-0.112}) \cdot 10^1$	$(^{+0.041}_{-0.034}) \cdot 10^1$
-0.80 – -0.60	5.078	± 0.793	$^{+0.323}_{-0.670}$	$^{+0.176}_{-0.105}$
-0.60 – -0.40	1.373	± 0.414	$^{+0.363}_{-0.552}$	$^{+0.042}_{-0.023}$

Table 2: The differential dijet cross section $d\sigma_{2+1}/d\log_{10}(x_{Bj})$. Other details are as described in the caption to Table 1.

$\log_{10}(\xi)$ range	$d\sigma_{2+1}/d\log_{10}(\xi)$ [pb]	$\Delta_{\rm stat}$	$\Delta_{\rm syst}$	$\Delta_{\rm ES}$
-2.1875 – -1.8750	3.386	± 0.939	$^{+0.970}_{-0.736}$	$^{+0.093}_{-0.078}$
-1.8750 – -1.5625	$2.726 \cdot 10^1$	$(\pm 0.179) \cdot 10^1$	$(^{+0.126}_{-0.045}) \cdot 10^1$	$(^{+0.021}_{-0.037}) \cdot 10^1$
-1.5625 – -1.2500	$6.379 \cdot 10^1$	$(\pm 0.266) \cdot 10^1$	$(^{+0.085}_{-0.334}) \cdot 10^1$	$(^{+0.147}_{-0.136}) \cdot 10^1$
-1.2500 – -0.9375	$5.997 \cdot 10^1$	$(\pm 0.260) \cdot 10^1$	$(^{+0.156}_{-0.224}) \cdot 10^1$	$(^{+0.199}_{-0.189}) \cdot 10^1$
-0.9375 – -0.6250	$2.232 \cdot 10^1$	$(\pm 0.142) \cdot 10^1$	$(^{+0.105}_{-0.154}) \cdot 10^1$	$(^{+0.126}_{-0.108}) \cdot 10^1$
-0.6250 – -0.3125	2.434	± 0.400	$^{+0.305}_{-0.229}$	$^{+0.177}_{-0.123}$

Table 3: The differential dijet cross section $d\sigma_{2+1}/d\log_{10}(\xi)$. Other details are as described in the caption to Table 1.

M_{jj} range [GeV]	$d\sigma_{2+1}/dM_{jj}$ [pb/GeV]	$\Delta_{\rm stat}$	$\Delta_{\rm syst}$	$\Delta_{\rm ES}$
10.00 – 16.00	$7.462 \cdot 10^{-1}$	$(\pm 0.642) \cdot 10^{-1}$	$(^{+0.562}_{-1.434}) \cdot 10^{-1}$	$(^{+0.016}_{-0.005}) \cdot 10^{-1}$
16.00 – 22.00	2.404	± 0.122	$^{+0.055}_{-0.055}$	$^{+0.034}_{-0.035}$
22.00 – 28.00	2.127	± 0.109	$^{+0.048}_{-0.041}$	$^{+0.057}_{-0.053}$
28.00 – 35.00	1.272	± 0.077	$^{+0.060}_{-0.038}$	$^{+0.046}_{-0.042}$
35.00 – 45.00	$7.494 \cdot 10^{-1}$	$(\pm 0.497) \cdot 10^{-1}$	$(^{+0.090}_{-0.309}) \cdot 10^{-1}$	$(^{+0.256}_{-0.246}) \cdot 10^{-1}$
45.00 – 60.00	$3.430 \cdot 10^{-1}$	$(\pm 0.284) \cdot 10^{-1}$	$(^{+0.100}_{-0.484}) \cdot 10^{-1}$	$(^{+0.270}_{-0.195}) \cdot 10^{-1}$
60.00 – 80.00	$9.605 \cdot 10^{-2}$	$(\pm 1.272) \cdot 10^{-2}$	$(^{+0.326}_{-0.419}) \cdot 10^{-2}$	$(^{+0.619}_{-0.709}) \cdot 10^{-2}$
80.00 – 120.00	$1.578 \cdot 10^{-2}$	$(\pm 0.353) \cdot 10^{-2}$	$(^{+0.122}_{-0.219}) \cdot 10^{-2}$	$(^{+0.117}_{-0.145}) \cdot 10^{-2}$

Table 4: The differential dijet cross section $d\sigma_{2+1}/dM_{jj}$. Other details are as described in the caption to Table 1.

$E_{T,B}^{jet,1}$ range [GeV]	$d\sigma_{2+1}/dE_{T,B}^{jet,1}$ [pb/GeV]	$\Delta_{\rm stat}$	$\Delta_{\rm syst}$	$\Delta_{\rm ES}$
5.00 – 8.00	2.956	± 0.175	$^{+0.154}_{-0.243}$	$^{+0.072}_{-0.081}$
8.00 – 12.00	5.977	± 0.238	$^{+0.105}_{-0.201}$	$^{+0.094}_{-0.090}$
12.00 – 16.00	2.736	± 0.154	$^{+0.039}_{-0.033}$	$^{+0.083}_{-0.081}$
16.00 – 20.00	1.327	± 0.103	$^{+0.055}_{-0.030}$	$^{+0.072}_{-0.026}$
20.00 – 24.00	$8.165 \cdot 10^{-1}$	$(\pm 0.801) \cdot 10^{-1}$	$(^{+0.096}_{-0.397}) \cdot 10^{-1}$	$(^{+0.245}_{-0.566}) \cdot 10^{-1}$
24.00 – 32.00	$2.848 \cdot 10^{-1}$	$(\pm 0.333) \cdot 10^{-1}$	$(^{+0.077}_{-0.355}) \cdot 10^{-1}$	$(^{+0.236}_{-0.183}) \cdot 10^{-1}$
32.00 – 50.00	$5.960 \cdot 10^{-2}$	$(\pm 0.879) \cdot 10^{-2}$	$(^{+0.997}_{-0.449}) \cdot 10^{-2}$	$(^{+0.572}_{-0.497}) \cdot 10^{-2}$
50.00 – 80.00	$3.991 \cdot 10^{-3}$	$(\pm 1.203) \cdot 10^{-3}$	$(^{+1.086}_{-0.902}) \cdot 10^{-3}$	$(^{+0.548}_{-0.472}) \cdot 10^{-3}$

Table 5: The differential dijet cross section $d\sigma_{2+1}/dE_{T,B}^{jet,1}$. Other details are as described in the caption to Table 1.

$\eta_B^{jet,1}$ range	$d\sigma_{2+1}/d\eta_B^{jet,1}$ [pb]	$\Delta_{\rm stat}$	$\Delta_{\rm syst}$	$\Delta_{\rm ES}$
-1.00 – -0.50	3.051	± 0.419	$^{+0.360}_{-0.277}$	$^{+0.155}_{-0.141}$
-0.50 – 0.00	$1.170 \cdot 10^1$	$(\pm 0.084) \cdot 10^1$	$(^{+0.025}_{-0.158}) \cdot 10^1$	$(^{+0.060}_{-0.051}) \cdot 10^1$
0.00 – 0.50	$3.260 \cdot 10^1$	$(\pm 0.154) \cdot 10^1$	$(^{+0.116}_{-0.105}) \cdot 10^1$	$(^{+0.102}_{-0.091}) \cdot 10^1$
0.50 – 1.00	$3.204 \cdot 10^1$	$(\pm 0.151) \cdot 10^1$	$(^{+0.084}_{-0.147}) \cdot 10^1$	$(^{+0.068}_{-0.075}) \cdot 10^1$
1.00 – 1.50	$2.054 \cdot 10^1$	$(\pm 0.119) \cdot 10^1$	$(^{+0.083}_{-0.104}) \cdot 10^1$	$(^{+0.046}_{-0.049}) \cdot 10^1$
1.50 – 2.00	9.035	± 0.748	$^{+0.570}_{-0.742}$	$^{+0.229}_{-0.194}$
2.00 – 2.50	2.561	± 0.410	$^{+0.491}_{-0.324}$	$^{+0.061}_{-0.058}$

Table 6: The differential dijet cross section $d\sigma_{2+1}/d\eta_B^{jet,1}$. Other details are as described in the caption to Table 1.

$E_{T,B}^{jet,2}$ range [GeV]	$d\sigma_{2+1}/dE_{T,B}^{jet,2}$ [pb/GeV]	$\Delta_{\rm stat}$	$\Delta_{\rm syst}$	$\Delta_{\rm ES}$
5.00 – 8.00	2.775	± 0.168	$^{+0.098}_{-0.235}$	$^{+0.074}_{-0.082}$
8.00 – 12.00	5.971	± 0.240	$^{+0.142}_{-0.154}$	$^{+0.103}_{-0.092}$
12.00 – 16.00	2.762	± 0.152	$^{+0.074}_{-0.071}$	$^{+0.088}_{-0.076}$
16.00 – 20.00	1.403	± 0.105	$^{+0.011}_{-0.034}$	$^{+0.062}_{-0.050}$
20.00 – 24.00	$7.437 \cdot 10^{-1}$	$(\pm 0.763) \cdot 10^{-1}$	$(^{+0.144}_{-1.274}) \cdot 10^{-1}$	$(^{+0.397}_{-0.406}) \cdot 10^{-1}$
24.00 – 32.00	$2.995 \cdot 10^{-1}$	$(\pm 0.339) \cdot 10^{-1}$	$(^{+0.070}_{-0.507}) \cdot 10^{-1}$	$(^{+0.182}_{-0.198}) \cdot 10^{-1}$
32.00 – 50.00	$6.834 \cdot 10^{-2}$	$(\pm 0.966) \cdot 10^{-2}$	$(^{+0.641}_{-0.239}) \cdot 10^{-2}$	$(^{+0.551}_{-0.452}) \cdot 10^{-2}$
50.00 – 80.00	$3.189 \cdot 10^{-3}$	$(\pm 1.205) \cdot 10^{-3}$	$(^{+0.981}_{-0.621}) \cdot 10^{-3}$	$(^{+0.203}_{-0.251}) \cdot 10^{-3}$

Table 7: The differential dijet cross section $d\sigma_{2+1}/dE_{T,B}^{jet,2}$. Other details are as described in the caption to Table 1.

$\eta_B^{jet,2}$ range	$d\sigma_{2+1}/d\eta_B^{jet,2}$ [pb]	$\Delta_{\rm stat}$	$\Delta_{\rm syst}$	$\Delta_{\rm ES}$
-2.00 – -1.50	2.507	± 0.458	$^{+0.219}_{-0.670}$	$^{+0.202}_{-0.190}$
-1.50 – -1.00	$1.054 \cdot 10^1$	$(\pm 0.084) \cdot 10^1$	$(^{+0.043}_{-0.084}) \cdot 10^1$	$(^{+0.069}_{-0.067}) \cdot 10^1$
-1.00 – -0.50	$3.328 \cdot 10^1$	$(\pm 0.151) \cdot 10^1$	$(^{+0.080}_{-0.170}) \cdot 10^1$	$(^{+0.154}_{-0.134}) \cdot 10^1$
-0.50 – 0.00	$3.735 \cdot 10^1$	$(\pm 0.163) \cdot 10^1$	$(^{+0.067}_{-0.130}) \cdot 10^1$	$(^{+0.073}_{-0.066}) \cdot 10^1$
0.00 – 0.50	$1.885 \cdot 10^1$	$(\pm 0.112) \cdot 10^1$	$(^{+0.062}_{-0.066}) \cdot 10^1$	$(^{+0.012}_{-0.014}) \cdot 10^1$
0.50 – 1.00	6.868	± 0.627	$^{+0.504}_{-0.252}$	$^{+0.070}_{-0.080}$
1.00 – 1.50	1.914	± 0.349	$^{+0.288}_{-0.273}$	$^{+0.066}_{-0.057}$

Table 8: The differential dijet cross section $d\sigma_{2+1}/d\eta_B^{jet,2}$. Other details are as described in the caption to Table 1.

Q^2 range [GeV^2]	$d\sigma_{\rm tot}/dQ^2$ [pb/GeV^2]	$\Delta_{\rm stat}$	$\Delta_{\rm syst}$
470. – 800.	1.217	± 0.011	$^{+0.015}_{-0.006}$
800. – 1500.	$2.800 \cdot 10^{-1}$	$(\pm 0.033) \cdot 10^{-1}$	$(^{+0.023}_{-0.019}) \cdot 10^{-1}$
1500. – 2500.	$6.509 \cdot 10^{-2}$	$(\pm 0.130) \cdot 10^{-2}$	$(^{+0.103}_{-0.090}) \cdot 10^{-2}$
2500. – 5000.	$1.230 \cdot 10^{-2}$	$(\pm 0.036) \cdot 10^{-2}$	$(^{+0.022}_{-0.020}) \cdot 10^{-2}$
5000. – 20000.	$7.378 \cdot 10^{-4}$	$(\pm 0.400) \cdot 10^{-4}$	$(^{+0.051}_{-0.163}) \cdot 10^{-4}$

Table 9: The differential inclusive cross section $d\sigma_{\rm tot}/dQ^2$. Other details are as described in the caption to Table 1.

Q^2 range [GeV^2]	$d\sigma_{2+1}/dQ^2$ [pb/GeV^2]	$\Delta_{\rm stat}$	$\Delta_{\rm syst}$	$\Delta_{\rm ES}$
470. – 800.	$8.061 \cdot 10^{-2}$	$(\pm 0.306) \cdot 10^{-2}$	$(^{+0.212}_{-0.294}) \cdot 10^{-2}$	$(^{+0.287}_{-0.256}) \cdot 10^{-2}$
800. – 1500.	$2.415 \cdot 10^{-2}$	$(\pm 0.105) \cdot 10^{-2}$	$(^{+0.039}_{-0.061}) \cdot 10^{-2}$	$(^{+0.071}_{-0.072}) \cdot 10^{-2}$
1500. – 2500.	$6.802 \cdot 10^{-3}$	$(\pm 0.453) \cdot 10^{-3}$	$(^{+0.300}_{-0.343}) \cdot 10^{-3}$	$(^{+0.159}_{-0.160}) \cdot 10^{-3}$
2500. – 5000.	$1.637 \cdot 10^{-3}$	$(\pm 0.139) \cdot 10^{-3}$	$(^{+0.046}_{-0.124}) \cdot 10^{-3}$	$(^{+0.033}_{-0.028}) \cdot 10^{-3}$
5000. – 20000.	$1.246 \cdot 10^{-4}$	$(\pm 0.170) \cdot 10^{-4}$	$(^{+0.006}_{-0.139}) \cdot 10^{-4}$	$(^{+0.013}_{-0.018}) \cdot 10^{-4}$

Table 10: The differential dijet cross section $d\sigma_{2+1}/dQ^2$. Other details are as described in the caption to Table 1.

Q^2 range [GeV^2]	R_{2+1}	$\Delta_{\rm stat}$	$\Delta_{\rm syst}$	$\Delta_{\rm ES}$
470. – 800.	$6.625 \cdot 10^{-2}$	$(\pm 0.245) \cdot 10^{-2}$	$(^{+0.168}_{-0.278}) \cdot 10^{-2}$	$(^{+0.236}_{-0.210}) \cdot 10^{-2}$
800. – 1500.	$8.627 \cdot 10^{-2}$	$(\pm 0.362) \cdot 10^{-2}$	$(^{+0.144}_{-0.267}) \cdot 10^{-2}$	$(^{+0.255}_{-0.256}) \cdot 10^{-2}$
1500. – 2500.	$1.045 \cdot 10^{-1}$	$(\pm 0.066) \cdot 10^{-1}$	$(^{+0.043}_{-0.057}) \cdot 10^{-1}$	$(^{+0.024}_{-0.025}) \cdot 10^{-1}$
2500. – 5000.	$1.331 \cdot 10^{-1}$	$(\pm 0.106) \cdot 10^{-1}$	$(^{+0.039}_{-0.119}) \cdot 10^{-1}$	$(^{+0.027}_{-0.023}) \cdot 10^{-1}$
5000. – 20000.	$1.688 \cdot 10^{-1}$	$(\pm 0.211) \cdot 10^{-1}$	$(^{+0.008}_{-0.185}) \cdot 10^{-1}$	$(^{+0.017}_{-0.024}) \cdot 10^{-1}$

Table 11: The dijet fraction $R_{2+1}(Q^2)$. Other details are as described in the caption to Table 1.

$z_{p,1}$ range	$< z_{p,1} >$	$d\sigma^{NLO}_{2+1}/dz_{p,1}$ [pb]	Δ_{μ_r}	Δ_{α_s}	$\Delta^{\rm exp}_{pdf}$	$\Delta^{\rm theo}_{pdf}$	$C_{\rm had} \pm \Delta C_{\rm had}$
0.00 – 0.05	0.04	$1.854 \cdot 10^1$	$(^{+0.256}_{-0.197}) \cdot 10^1$	$(^{+0.147}_{-0.143}) \cdot 10^1$	$(\pm 0.105) \cdot 10^1$	$(^{+0.023}_{-0.027}) \cdot 10^1$	1.38± 0.04
0.05 – 0.15	0.10	$1.172 \cdot 10^2$	$(^{+0.100}_{-0.088}) \cdot 10^2$	$(^{+0.078}_{-0.082}) \cdot 10^2$	$(\pm 0.060) \cdot 10^2$	$(^{+0.014}_{-0.014}) \cdot 10^2$	1.10± 0.01
0.15 – 0.25	0.20	$1.167 \cdot 10^2$	$(^{+0.056}_{-0.062}) \cdot 10^2$	$(^{+0.070}_{-0.075}) \cdot 10^2$	$(\pm 0.067) \cdot 10^2$	$(^{+0.015}_{-0.014}) \cdot 10^2$	1.08± 0.04
0.25 – 0.35	0.30	$9.100 \cdot 10^1$	$(^{+0.351}_{-0.432}) \cdot 10^1$	$(^{+0.542}_{-0.577}) \cdot 10^1$	$(\pm 0.529) \cdot 10^1$	$(^{+0.120}_{-0.118}) \cdot 10^1$	1.07± 0.01
0.35 – 0.45	0.40	$7.481 \cdot 10^1$	$(^{+0.280}_{-0.349}) \cdot 10^1$	$(^{+0.454}_{-0.477}) \cdot 10^1$	$(\pm 0.421) \cdot 10^1$	$(^{+0.100}_{-0.097}) \cdot 10^1$	1.07± 0.02
0.45 – 0.55	0.50	$6.667 \cdot 10^1$	$(^{+0.275}_{-0.327}) \cdot 10^1$	$(^{+0.403}_{-0.425}) \cdot 10^1$	$(\pm 0.361) \cdot 10^1$	$(^{+0.089}_{-0.085}) \cdot 10^1$	1.09± 0.02
0.55 – 0.65	0.60	$5.711 \cdot 10^1$	$(^{+0.185}_{-0.250}) \cdot 10^1$	$(^{+0.339}_{-0.356}) \cdot 10^1$	$(\pm 0.349) \cdot 10^1$	$(^{+0.074}_{-0.070}) \cdot 10^1$	1.09± 0.01
0.65 – 0.75	0.70	$4.858 \cdot 10^1$	$(^{+0.219}_{-0.248}) \cdot 10^1$	$(^{+0.294}_{-0.308}) \cdot 10^1$	$(\pm 0.309) \cdot 10^1$	$(^{+0.061}_{-0.058}) \cdot 10^1$	1.15± 0.03
0.75 – 0.85	0.79	$2.776 \cdot 10^1$	$(^{+0.215}_{-0.194}) \cdot 10^1$	$(^{+0.202}_{-0.193}) \cdot 10^1$	$(\pm 0.168) \cdot 10^1$	$(^{+0.037}_{-0.036}) \cdot 10^1$	1.28± 0.00
0.85 – 0.95	0.88	4.466	$^{+0.573}_{-0.445}$	$^{+0.377}_{-0.318}$	± 0.265	$^{+0.049}_{-0.072}$	1.27± 0.13

Table 12: The QCD predictions for the differential dijet cross section as a function of $z_{p,1}$. For each bin in $z_{p,1}$ the following quantities are given: the weighted mean value $< z_{p,1} >$, the pure NLO QCD cross section, the uncertainty due to the renormalization scale, Δ_{μ_r}, the uncertainty due to $\alpha_s(M_Z)$, Δ_{α_s}, the uncertainty due to the proton PDFs (experimental), $\Delta^{\rm exp}_{pdf}$, the uncertainty due to the proton PDFs (theoretical), $\Delta^{\rm theo}_{pdf}$, and the hadronisation correction, $C_{\rm had}$, with its associated uncertainty, $\Delta C_{\rm had}$.

$\log_{10}(x_{Bj})$ range	$<\log_{10}(x_{Bj})>$	$d\sigma^{NLO}_{2+1}/d\log_{10}(x_{Bj})$ [pb]	Δ_{μ_r}	Δ_{α_s}	$\Delta^{\rm exp}_{pdf}$	$\Delta^{\rm theo}_{pdf}$	$C_{\rm had} \pm \Delta C_{\rm had}$
-2.2 – -2.0	-2.08	$2.509 \cdot 10^1$	$^{(+0.184}_{-0.173)} \cdot 10^1$	$^{(+0.121}_{-0.157)} \cdot 10^1$	$(\pm 0.140) \cdot 10^1$	$^{(+0.036}_{-0.040)} \cdot 10^1$	1.04± 0.02
-2.0 – -1.8	-1.90	$5.025 \cdot 10^1$	$^{(+0.285}_{-0.297)} \cdot 10^1$	$^{(+0.246}_{-0.311)} \cdot 10^1$	$(\pm 0.248) \cdot 10^1$	$^{(+0.064}_{-0.072)} \cdot 10^1$	1.06± 0.01
-1.8 – -1.6	-1.70	$6.477 \cdot 10^1$	$^{(+0.336}_{-0.361)} \cdot 10^1$	$^{(+0.363}_{-0.419)} \cdot 10^1$	$(\pm 0.256) \cdot 10^1$	$^{(+0.076}_{-0.078)} \cdot 10^1$	1.08± 0.02
-1.6 – -1.4	-1.50	$6.403 \cdot 10^1$	$^{(+0.311}_{-0.341)} \cdot 10^1$	$^{(+0.423}_{-0.436)} \cdot 10^1$	$(\pm 0.205) \cdot 10^1$	$^{(+0.079}_{-0.068)} \cdot 10^1$	1.10± 0.01
-1.4 – -1.2	-1.31	$5.003 \cdot 10^1$	$^{(+0.247}_{-0.266)} \cdot 10^1$	$^{(+0.377}_{-0.353)} \cdot 10^1$	$(\pm 0.165) \cdot 10^1$	$^{(+0.072}_{-0.059)} \cdot 10^1$	1.14± 0.01
-1.2 – -1.0	-1.11	$2.935 \cdot 10^1$	$^{(+0.148}_{-0.155)} \cdot 10^1$	$^{(+0.231}_{-0.201)} \cdot 10^1$	$(\pm 0.122) \cdot 10^1$	$^{(+0.044}_{-0.037)} \cdot 10^1$	1.15± 0.02
-1.0 – -0.8	-0.91	$1.391 \cdot 10^1$	$^{(+0.070}_{-0.071)} \cdot 10^1$	$^{(+0.100}_{-0.083)} \cdot 10^1$	$(\pm 0.064) \cdot 10^1$	$^{(+0.017}_{-0.017)} \cdot 10^1$	1.13± 0.01
-0.8 – -0.6	-0.72	5.604	$^{+0.283}_{-0.282}$	$^{+0.322}_{-0.263}$	±0.244	$^{+0.041}_{-0.069}$	1.11± 0.01
-0.6 – -0.4	-0.52	1.650	$^{+0.088}_{-0.082}$	$^{+0.061}_{-0.051}$	±0.062	$^{+0.000}_{-0.023}$	1.14± 0.05

Table 13: The QCD predictions for the differential dijet cross section as a function of $\log_{10}(x_{Bj})$. Other details are as described in the caption to Table 12.

$\log_{10}(\xi)$ range	$<\log_{10}(\xi)>$	$d\sigma^{NLO}_{2+1}/d\log_{10}(\xi)$ [pb]	Δ_{μ_r}	Δ_{α_s}	$\Delta^{\rm exp}_{pdf}$	$\Delta^{\rm theo}_{pdf}$	$C_{\rm had} \pm \Delta C_{\rm had}$
-2.1875 – -1.8750	-1.94	2.825	$^{+0.737}_{-0.503}$	$^{+0.233}_{-0.258}$	±0.166	$^{+0.047}_{-0.051}$	1.18± 0.05
-1.8750 – -1.5625	-1.68	$2.951 \cdot 10^1$	$^{(+0.363}_{-0.290)} \cdot 10^1$	$^{(+0.167}_{-0.205)} \cdot 10^1$	$(\pm 0.180) \cdot 10^1$	$^{(+0.043}_{-0.048)} \cdot 10^1$	1.09± 0.01
-1.5625 – -1.2500	-1.40	$6.736 \cdot 10^1$	$^{(+0.416}_{-0.416)} \cdot 10^1$	$^{(+0.372}_{-0.434)} \cdot 10^1$	$(\pm 0.318) \cdot 10^1$	$^{(+0.075}_{-0.076)} \cdot 10^1$	1.06± 0.01
-1.2500 – -0.9375	-1.11	$6.746 \cdot 10^1$	$^{(+0.198}_{-0.282)} \cdot 10^1$	$^{(+0.453}_{-0.448)} \cdot 10^1$	$(\pm 0.273) \cdot 10^1$	$^{(+0.085}_{-0.069)} \cdot 10^1$	1.11± 0.01
-0.9375 – -0.6250	-0.82	$2.569 \cdot 10^1$	$^{(+0.002}_{-0.059)} \cdot 10^1$	$^{(+0.190}_{-0.157)} \cdot 10^1$	$(\pm 0.162) \cdot 10^1$	$^{(+0.041}_{-0.040)} \cdot 10^1$	1.14± 0.02
-0.6250 – -0.3125	-0.53	3.378	$^{+0.000}_{-0.059}$	$^{+0.177}_{-0.122}$	±0.220	$^{+0.027}_{-0.067}$	1.11± 0.06

Table 14: The QCD predictions for the differential dijet cross section as a function of $\log_{10}(\xi)$. Other details are as described in the caption to Table 12.

M_{jj} range [GeV]	$< M_{jj} >$	$d\sigma_{2+1}^{NLO}/dM_{jj}$ [pb/GeV]	Δ_{μ_r}	Δ_{α_s}	$\Delta_{pdf}^{\rm exp}$	$\Delta_{pdf}^{\rm theo}$	$C_{\rm had} \pm \Delta C_{\rm had}$
10. – 16.	14.65	$6.351 \cdot 10^{-1}$	$(^{+2.017}_{-1.355}) \cdot 10^{-1}$	$(^{+0.751}_{-0.684}) \cdot 10^{-1}$	$(\pm 0.190) \cdot 10^{-1}$	$(^{+0.099}_{-0.112}) \cdot 10^{-1}$	1.16± 0.02
16. – 22.	19.03	2.914	$^{+0.346}_{-0.278}$	$^{+0.208}_{-0.216}$	±0.149	$^{+0.038}_{-0.036}$	1.14± 0.03
22. – 28.	24.98	2.331	$^{+0.079}_{-0.104}$	$^{+0.126}_{-0.141}$	±0.161	$^{+0.028}_{-0.026}$	1.13± 0.02
28. – 35.	31.32	1.487	$^{+0.000}_{-0.035}$	$^{+0.073}_{-0.083}$	±0.112	$^{+0.017}_{-0.016}$	1.05± 0.01
35. – 45.	39.42	$8.119 \cdot 10^{-1}$	$(^{+0.000}_{-0.174}) \cdot 10^{-1}$	$(^{+0.403}_{-0.446}) \cdot 10^{-1}$	$(\pm 0.567) \cdot 10^{-1}$	$(^{+0.095}_{-0.091}) \cdot 10^{-1}$	1.04± 0.02
45. – 60.	51.11	$3.227 \cdot 10^{-1}$	$(^{+0.000}_{-0.111}) \cdot 10^{-1}$	$(^{+0.174}_{-0.179}) \cdot 10^{-1}$	$(\pm 0.223) \cdot 10^{-1}$	$(^{+0.042}_{-0.041}) \cdot 10^{-1}$	1.00± 0.02
60. – 80.	67.73	$9.154 \cdot 10^{-2}$	$(^{+0.216}_{-0.712}) \cdot 10^{-2}$	$(^{+0.553}_{-0.493}) \cdot 10^{-2}$	$(\pm 0.767) \cdot 10^{-2}$	$(^{+0.155}_{-0.164}) \cdot 10^{-2}$	1.05± 0.02
80. – 120.	92.06	$1.657 \cdot 10^{-2}$	$(^{+0.072}_{-0.182}) \cdot 10^{-2}$	$(^{+0.128}_{-0.091}) \cdot 10^{-2}$	$(\pm 0.170) \cdot 10^{-2}$	$(^{+0.040}_{-0.050}) \cdot 10^{-2}$	0.96± 0.02

Table 15: The QCD predictions for the differential dijet cross section as a function of M_{jj}. Other details are as described in the caption to Table 12.

$E_{TB}^{jet,1}$ range [GeV]	$< E_{T,B}^{jet,1} >$	$d\sigma_{2+1}^{NLO}/dE_{T,B}^{jet,1}$ [pb/GeV]	Δ_{μ_r}	Δ_{α_s}	$\Delta_{pdf}^{\rm exp}$	$\Delta_{pdf}^{\rm theo}$	$C_{\rm had} \pm \Delta C_{\rm had}$
5. – 8.	7.06	3.722	$^{+1.174}_{-0.790}$	$^{+0.429}_{-0.397}$	±0.108	$^{+0.056}_{-0.062}$	1.10± 0.01
8. – 12.	9.72	6.637	$^{+0.023}_{-0.176}$	$^{+0.304}_{-0.366}$	±0.407	$^{+0.075}_{-0.065}$	1.16± 0.03
12. – 16.	13.77	2.905	$^{+0.000}_{-0.067}$	$^{+0.145}_{-0.163}$	±0.190	$^{+0.034}_{-0.031}$	1.04± 0.00
16. – 20.	17.83	1.420	$^{+0.000}_{-0.030}$	$^{+0.079}_{-0.083}$	±0.096	$^{+0.018}_{-0.019}$	1.01± 0.01
20. – 24.	21.92	$7.071 \cdot 10^{-1}$	$(^{+0.000}_{-0.218}) \cdot 10^{-1}$	$(^{+0.426}_{-0.411}) \cdot 10^{-1}$	$(\pm 0.535) \cdot 10^{-1}$	$(^{+0.105}_{-0.107}) \cdot 10^{-1}$	1.00± 0.03
24. – 32.	27.28	$2.951 \cdot 10^{-1}$	$(^{+0.001}_{-0.118}) \cdot 10^{-1}$	$(^{+0.199}_{-0.175}) \cdot 10^{-1}$	$(\pm 0.214) \cdot 10^{-1}$	$(^{+0.051}_{-0.056}) \cdot 10^{-1}$	1.01± 0.03
32. – 50.	37.77	$5.730 \cdot 10^{-2}$	$(^{+0.098}_{-0.381}) \cdot 10^{-2}$	$(^{+0.464}_{-0.339}) \cdot 10^{-2}$	$(\pm 0.482) \cdot 10^{-2}$	$(^{+0.128}_{-0.173}) \cdot 10^{-2}$	1.01± 0.03
50. – 80.	57.65	$3.908 \cdot 10^{-3}$	$(^{+0.280}_{-0.609}) \cdot 10^{-3}$	$(^{+0.324}_{-0.162}) \cdot 10^{-3}$	$(\pm 0.441) \cdot 10^{-3}$	$(^{+0.094}_{-0.244}) \cdot 10^{-3}$	1.04± 0.03

Table 16: The QCD predictions for the differential dijet cross section as a function of $E_{TB}^{jet,1}$. Other details are as described in the caption to Table 12.

$\eta_B^{jet,1}$ range	$< \eta_B^{jet,1} >$	$d\sigma_{2+1}^{NLO}/d\eta_B^{jet,1}$ [pb]	Δ_{μ_r}	Δ_{α_s}	$\Delta_{pdf}^{\rm exp}$	$\Delta_{pdf}^{\rm theo}$	$C_{\rm had} \pm \Delta C_{\rm had}$
-1.0 – -0.5	-0.68	5.156	$^{+0.305}_{-0.294}$	$^{+0.335}_{-0.316}$	± 0.257	$^{+0.054}_{-0.046}$	1.47± 0.05
-0.5 – 0.0	-0.21	$1.972 \cdot 10^1$	$(^{+0.066}_{-0.086}) \cdot 10^1$	$(^{+0.115}_{-0.120}) \cdot 10^1$	$(\pm 0.109) \cdot 10^1$	$(^{+0.024}_{-0.022}) \cdot 10^1$	1.34± 0.05
0.0 – 0.5	0.26	$3.596 \cdot 10^1$	$(^{+0.126}_{-0.163}) \cdot 10^1$	$(^{+0.205}_{-0.222}) \cdot 10^1$	$(\pm 0.197) \cdot 10^1$	$(^{+0.046}_{-0.044}) \cdot 10^1$	1.11± 0.01
0.5 – 1.0	0.73	$3.136 \cdot 10^1$	$(^{+0.152}_{-0.168}) \cdot 10^1$	$(^{+0.194}_{-0.205}) \cdot 10^1$	$(\pm 0.171) \cdot 10^1$	$(^{+0.041}_{-0.041}) \cdot 10^1$	1.02± 0.02
1.0 – 1.5	1.22	$1.888 \cdot 10^1$	$(^{+0.144}_{-0.132}) \cdot 10^1$	$(^{+0.129}_{-0.134}) \cdot 10^1$	$(\pm 0.099) \cdot 10^1$	$(^{+0.025}_{-0.026}) \cdot 10^1$	0.99± 0.04
1.5 – 2.0	1.71	8.064	$^{+0.884}_{-0.724}$	$^{+0.596}_{-0.617}$	± 0.413	$^{+0.106}_{-0.112}$	1.00± 0.01
2.0 – 2.5	2.18	2.406	$^{+0.384}_{-0.287}$	$^{+0.197}_{-0.204}$	± 0.120	$^{+0.031}_{-0.033}$	1.08± 0.01

Table 17: The QCD predictions for the differential dijet cross section as a function of $\eta_B^{jet,1}$. Other details are as described in the caption to Table 12.

$E_{TB}^{jet,2}$ range [GeV]	$< E_{T,B}^{jet,2} >$	$d\sigma_{2+1}^{NLO}/dE_{T,B}^{jet,2}$ [pb/GeV]	Δ_{μ_r}	Δ_{α_s}	$\Delta_{pdf}^{\rm exp}$	$\Delta_{pdf}^{\rm theo}$	$C_{\rm had} \pm \Delta C_{\rm had}$
5. – 8.	7.10	3.623	$^{+1.148}_{-0.771}$	$^{+0.425}_{-0.390}$	± 0.109	$^{+0.056}_{-0.063}$	1.20± 0.02
8. – 12.	9.69	6.737	$^{+0.053}_{-0.196}$	$^{+0.315}_{-0.376}$	± 0.398	$^{+0.076}_{-0.066}$	1.13± 0.02
12. – 16.	13.75	2.877	$^{+0.000}_{-0.062}$	$^{+0.139}_{-0.159}$	± 0.185	$^{+0.033}_{-0.031}$	1.04± 0.01
16. – 20.	17.70	1.367	$^{+0.000}_{-0.033}$	$^{+0.071}_{-0.076}$	± 0.094	$^{+0.017}_{-0.016}$	1.02± 0.02
20. – 24.	21.70	$7.527 \cdot 10^{-1}$	$(^{+0.000}_{-0.154}) \cdot 10^{-1}$	$(^{+0.464}_{-0.455}) \cdot 10^{-1}$	$(\pm 0.527) \cdot 10^{-1}$	$(^{+0.106}_{-0.108}) \cdot 10^{-1}$	1.00± 0.03
24. – 32.	27.18	$3.020 \cdot 10^{-1}$	$(^{+0.000}_{-0.098}) \cdot 10^{-1}$	$(^{+0.210}_{-0.184}) \cdot 10^{-1}$	$(\pm 0.212) \cdot 10^{-1}$	$(^{+0.052}_{-0.057}) \cdot 10^{-1}$	0.99± 0.03
32. – 50.	37.71	$5.643 \cdot 10^{-2}$	$(^{+0.117}_{-0.410}) \cdot 10^{-2}$	$(^{+0.446}_{-0.327}) \cdot 10^{-2}$	$(\pm 0.476) \cdot 10^{-2}$	$(^{+0.125}_{-0.165}) \cdot 10^{-2}$	1.02± 0.03
50. – 80.	57.61	$3.867 \cdot 10^{-3}$	$(^{+0.288}_{-0.618}) \cdot 10^{-3}$	$(^{+0.315}_{-0.161}) \cdot 10^{-3}$	$(\pm 0.440) \cdot 10^{-3}$	$(^{+0.093}_{-0.225}) \cdot 10^{-3}$	0.97± 0.03

Table 18: The QCD predictions for the differential dijet cross section as a function of $E_{TB}^{jet,2}$. Other details are as described in the caption to Table 12.

$\eta_B^{jet,2}$ range	$<\eta_B^{jet,2}>$	$d\sigma_{2+1}^{NLO}/d\eta_B^{jet,2}$ [pb]	Δ_{μ_r}	Δ_{α_s}	$\Delta_{pdf}^{\rm exp}$	$\Delta_{pdf}^{\rm theo}$	$C_{\rm had} \pm \Delta C_{\rm had}$
-2.0 – -1.5	-1.69	4.973	$^{+0.354}_{-0.317}$	$^{+0.343}_{-0.309}$	± 0.264	$^{+0.054}_{-0.051}$	1.51± 0.05
-1.5 – -1.0	-1.20	$1.972 \cdot 10^1$	$(^{+0.151}_{-0.135}) \cdot 10^1$	$(^{+0.135}_{-0.133}) \cdot 10^1$	$(\pm 0.104) \cdot 10^1$	$(^{+0.024}_{-0.022}) \cdot 10^1$	1.40± 0.00
-1.0 – -0.5	-0.74	$4.169 \cdot 10^1$	$(^{+0.154}_{-0.194}) \cdot 10^1$	$(^{+0.234}_{-0.258}) \cdot 10^1$	$(\pm 0.238) \cdot 10^1$	$(^{+0.051}_{-0.048}) \cdot 10^1$	1.21± 0.03
-0.5 – 0.0	-0.28	$3.427 \cdot 10^1$	$(^{+0.132}_{-0.164}) \cdot 10^1$	$(^{+0.195}_{-0.216}) \cdot 10^1$	$(\pm 0.180) \cdot 10^1$	$(^{+0.044}_{-0.043}) \cdot 10^1$	0.99± 0.02
0.0 – 0.5	0.20	$1.558 \cdot 10^1$	$(^{+0.100}_{-0.099}) \cdot 10^1$	$(^{+0.109}_{-0.110}) \cdot 10^1$	$(\pm 0.077) \cdot 10^1$	$(^{+0.023}_{-0.024}) \cdot 10^1$	0.92± 0.01
0.5 – 1.0	0.69	4.185	$^{+0.459}_{-0.377}$	$^{+0.371}_{-0.342}$	± 0.209	$^{+0.071}_{-0.079}$	0.96± 0.00
1.0 – 1.5	1.19	$9.857 \cdot 10^{-1}$	$(^{+2.051}_{-1.459}) \cdot 10^{-1}$	$(^{+1.041}_{-0.945}) \cdot 10^{-1}$	$(\pm 0.454) \cdot 10^{-1}$	$(^{+0.170}_{-0.201}) \cdot 10^{-1}$	1.36± 0.03

Table 19: The QCD predictions for the differential dijet cross section as a function of $\eta_B^{jet,2}$. Other details are as described in the caption to Table 12.

Q^2 range [GeV^2]	$<Q^2>$	$d\sigma_{tot}^{NLO}/dQ^2$ [pb/GeV^2]	Δ_{μ_r}	Δ_{α_s}	$\Delta_{pdf}^{\rm exp}$	$\Delta_{pdf}^{\rm theo}$
470. – 800.	599.	1.180	$^{+0.008}_{-0.011}$	$^{+0.002}_{-0.006}$	± 0.032	$^{+0.017}_{-0.014}$
800. – 1500.	1059.	$2.756 \cdot 10^{-1}$	$(^{+0.016}_{-0.021}) \cdot 10^{-1}$	$(^{+0.006}_{-0.012}) \cdot 10^{-1}$	$(\pm 0.067) \cdot 10^{-1}$	$(^{+0.034}_{-0.026}) \cdot 10^{-1}$
1500. – 2500.	1890.	$6.282 \cdot 10^{-2}$	$(^{+0.028}_{-0.036}) \cdot 10^{-2}$	$(^{+0.014}_{-0.015}) \cdot 10^{-2}$	$(\pm 0.146) \cdot 10^{-2}$	$(^{+0.064}_{-0.046}) \cdot 10^{-2}$
2500. – 5000.	3363.	$1.257 \cdot 10^{-2}$	$(^{+0.004}_{-0.005}) \cdot 10^{-2}$	$(^{+0.001}_{-0.000}) \cdot 10^{-2}$	$(\pm 0.030) \cdot 10^{-2}$	$(^{+0.009}_{-0.007}) \cdot 10^{-2}$
5000. – 20000.	7801.	$7.003 \cdot 10^{-4}$	$(^{+0.010}_{-0.012}) \cdot 10^{-4}$	$(^{+0.057}_{-0.035}) \cdot 10^{-4}$	$(\pm 0.188) \cdot 10^{-4}$	$(^{+0.003}_{-0.031}) \cdot 10^{-4}$

Table 20: The QCD predictions for the differential inclusive cross section as a function of Q^2. Other details are as described in the caption to Table 12.

Q^2 range [GeV^2]	$< Q^2 >$	$d\sigma_{2+1}^{NLO}/dQ^2$ [pb/GeV^2]	Δ_{μ_r}	Δ_{α_s}	$\Delta_{pdf}^{\rm exp}$	$\Delta_{pdf}^{\rm theo}$	$C_{\rm had} \pm \Delta C_{\rm had}$
470. – 800.	604.	$8.985 \cdot 10^{-2}$	$^{+0.583}_{-0.577}) \cdot 10^{-2}$	$^{+0.539}_{-0.606}) \cdot 10^{-2}$	$(\pm 0.388) \cdot 10^{-2}$	$^{+0.118}_{-0.121}) \cdot 10^{-2}$	1.11± 0.01
800. – 1500.	1071.	$2.597 \cdot 10^{-2}$	$^{+0.128}_{-0.139}) \cdot 10^{-2}$	$^{+0.167}_{-0.172}) \cdot 10^{-2}$	$(\pm 0.098) \cdot 10^{-2}$	$^{+0.034}_{-0.031}) \cdot 10^{-2}$	1.09± 0.01
1500. – 2500.	1901.	$7.208 \cdot 10^{-3}$	$^{+0.270}_{-0.324}) \cdot 10^{-3}$	$^{+0.484}_{-0.460}) \cdot 10^{-3}$	$(\pm 0.263) \cdot 10^{-3}$	$^{+0.095}_{-0.080}) \cdot 10^{-3}$	1.07± 0.01
2500. – 5000.	3420.	$1.734 \cdot 10^{-3}$	$^{+0.051}_{-0.067}) \cdot 10^{-3}$	$^{+0.114}_{-0.101}) \cdot 10^{-3}$	$(\pm 0.070) \cdot 10^{-3}$	$^{+0.022}_{-0.019}) \cdot 10^{-3}$	1.05± 0.01
5000. – 20000.	8095.	$1.281 \cdot 10^{-4}$	$^{+0.038}_{-0.046}) \cdot 10^{-4}$	$^{+0.068}_{-0.057}) \cdot 10^{-4}$	$(\pm 0.055) \cdot 10^{-4}$	$^{+0.008}_{-0.014}) \cdot 10^{-4}$	1.04± 0.01

Table 21: The QCD predictions for the differential dijet cross section as a function of Q^2. Other details are as described in the caption to Table 12.

Q^2 range [GeV^2]	$< Q^2 >$	R_{2+1}	Δ_{μ_r}	Δ_{α_s}	$\Delta_{pdf}^{\rm exp}$	$\Delta_{pdf}^{\rm theo}$	$C_{\rm had} \pm \Delta C_{\rm had}$
470. – 800.	604.	$7.615 \cdot 10^{-2}$	$^{+0.569}_{-0.538}) \cdot 10^{-2}$	$^{+0.443}_{-0.475}) \cdot 10^{-2}$	$(\pm 0.122) \cdot 10^{-2}$	$^{+0.000}_{-0.017}) \cdot 10^{-2}$	1.11± 0.01
800. – 1500.	1071.	$9.424 \cdot 10^{-2}$	$^{+0.539}_{-0.556}) \cdot 10^{-2}$	$^{+0.583}_{-0.586}) \cdot 10^{-2}$	$(\pm 0.122) \cdot 10^{-2}$	$^{+0.007}_{-0.025}) \cdot 10^{-2}$	1.09± 0.01
1500. – 2500.	1901.	$1.148 \cdot 10^{-1}$	$^{+0.050}_{-0.056}) \cdot 10^{-1}$	$^{+0.074}_{-0.071}) \cdot 10^{-1}$	$(\pm 0.015) \cdot 10^{-1}$	$^{+0.003}_{-0.004}) \cdot 10^{-1}$	1.07± 0.01
2500. – 5000.	3420.	$1.380 \cdot 10^{-1}$	$^{+0.047}_{-0.058}) \cdot 10^{-1}$	$^{+0.089}_{-0.081}) \cdot 10^{-1}$	$(\pm 0.022) \cdot 10^{-1}$	$^{+0.007}_{-0.007}) \cdot 10^{-1}$	1.05± 0.01
5000. – 20000.	8095.	$1.829 \cdot 10^{-1}$	$^{+0.057}_{-0.069}) \cdot 10^{-1}$	$^{+0.106}_{-0.096}) \cdot 10^{-1}$	$(\pm 0.029) \cdot 10^{-1}$	$^{+0.011}_{-0.012}) \cdot 10^{-1}$	1.04± 0.01

Table 22: The QCD predictions for the dijet fraction as a function of Q^2. Other details are as described in the caption to Table 12.

$\langle Q \rangle$ [GeV]	$\alpha_s(\langle Q \rangle)$	$\Delta\alpha_s^{\rm stat}$	$\Delta\alpha_s^{\rm syst}$	$\Delta\alpha_s^{\rm ES}$	$\Delta\alpha_s^{\rm Th}$
24.6	0.1436	0.0047	$^{+0.0032}_{-0.0066}$	$^{+0.0045}_{-0.0041}$	$^{+0.0105}_{-0.0079}$
32.7	0.1396	0.0048	$^{+0.0019}_{-0.0036}$	$^{+0.0034}_{-0.0034}$	$^{+0.0078}_{-0.0059}$
43.6	0.1306	0.0063	$^{+0.0041}_{-0.0044}$	$^{+0.0023}_{-0.0024}$	$^{+0.0054}_{-0.0040}$
58.5	0.1276	0.0075	$^{+0.0027}_{-0.0041}$	$^{+0.0019}_{-0.0016}$	$^{+0.0046}_{-0.0033}$
90.0	0.1149	0.0111	$^{+0.0056}_{-0.0099}$	$^{+0.0009}_{-0.0013}$	$^{+0.0037}_{-0.0028}$

Table 23: The α_s values as determined from the QCD fit to the measured dijet fraction R_{2+1} as a function of Q. For each bin in Q^2, the mean value $\langle Q \rangle$, the extracted value of the strong coupling constant, $\alpha_s(\langle Q \rangle)$, the statistical uncertainty, $\Delta\alpha_s^{\rm stat}$, the systematic uncertainty (not) associated with the energy scale of the jets, $\Delta\alpha_s^{\rm ES}$ ($\Delta\alpha_s^{\rm syst}$), and the total theoretical uncertainty, $\Delta\alpha_s^{\rm Th}$, are given.

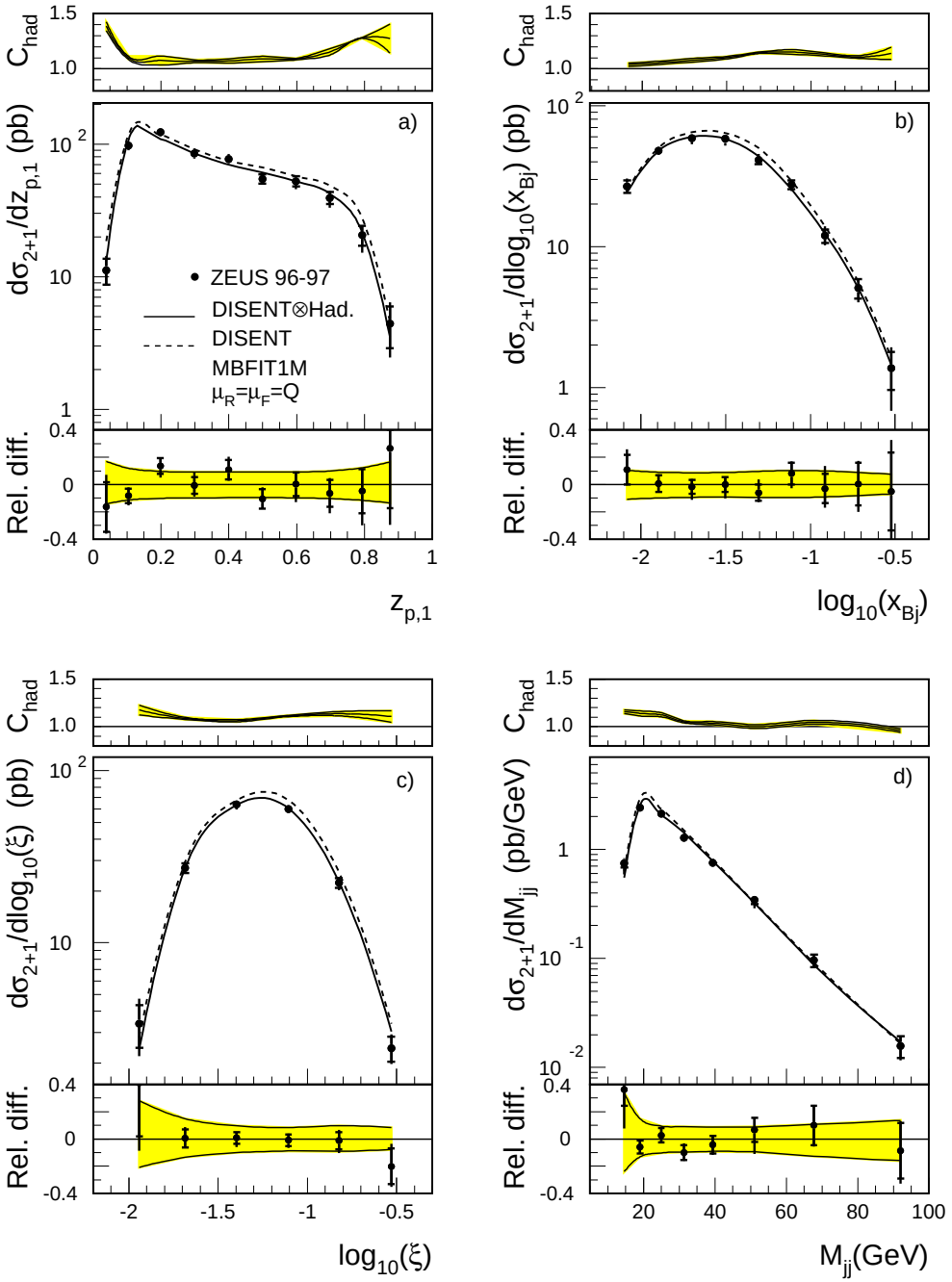

Figure 1: The measured differential dijet cross sections in NC DIS as functions of a) $z_{p,1}$, b) $\log_{10} x_{Bj}$, c) $\log_{10} \xi$ and d) dijet invariant mass M_{jj}. The inner error bars represent the statistical errors of the data. The outer error bars show the statistical errors and systematic uncertainties − except those associated with the uncertainty in the absolute energy scale of the jets − added in quadrature. For comparison, pure NLO QCD calculations (dashed lines) and NLO QCD calculations corrected for hadronisation effects (solid lines), obtained using the proton MBFIT PDFs and $\mu_R = \mu_F = Q$, are shown. The relative differences of the measured differential cross sections over the NLO QCD predictions corrected for hadronisation effects are shown underneath each plot; the shaded band represents the uncertainty of the QCD calculation (see text). The hadronisation correction ($C_{\rm had}$) together with its uncertainty are shown above each plot.

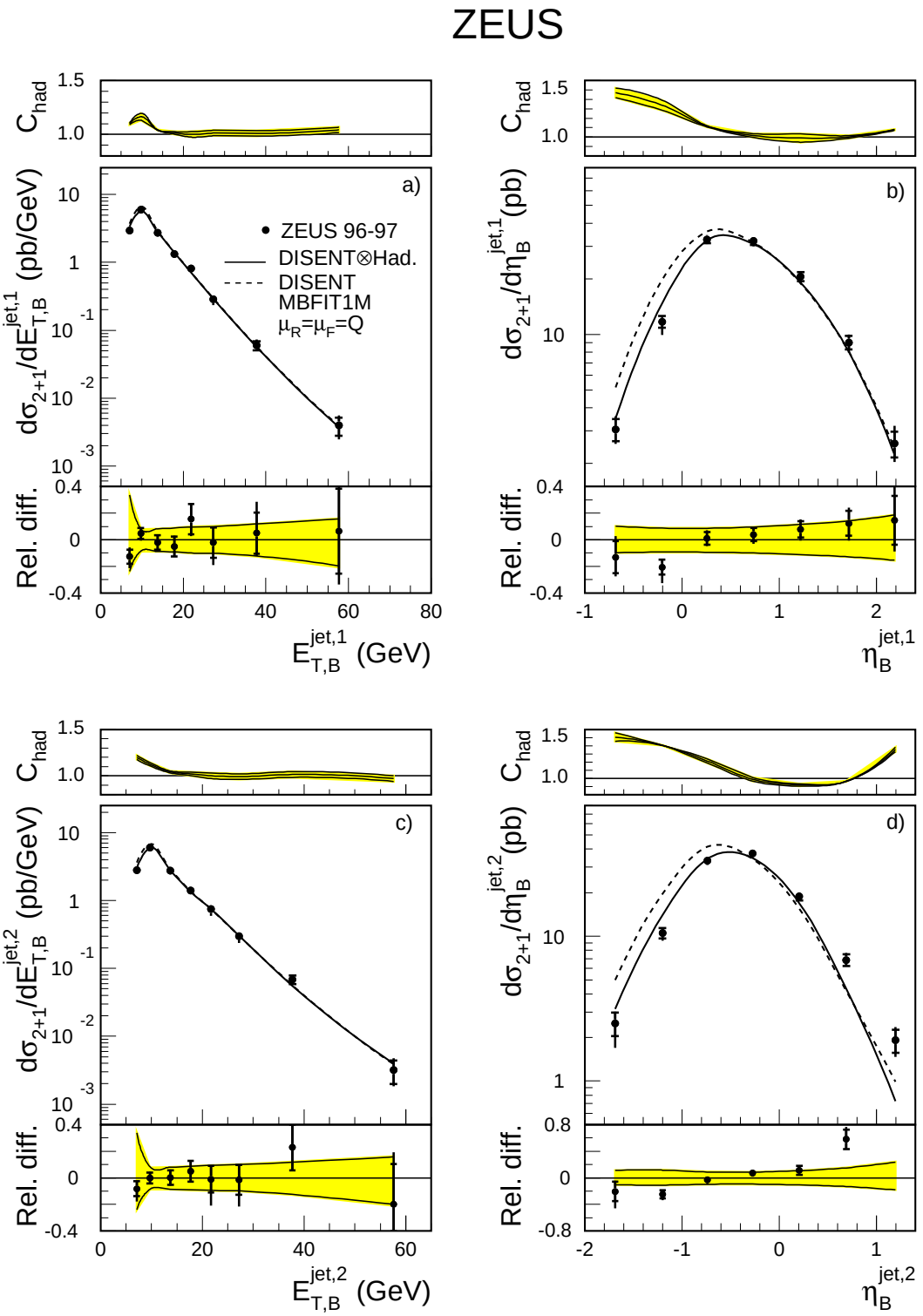

Figure 2: The measured differential dijet cross sections in NC DIS as functions of a) $E_{T,B}^{\mathrm{jet},1}$, b) $\eta_B^{\mathrm{jet},1}$, c) $E_{T,B}^{\mathrm{jet},2}$ and d) $\eta_B^{\mathrm{jet},2}$. Other details are as described in the caption to Fig. 1.

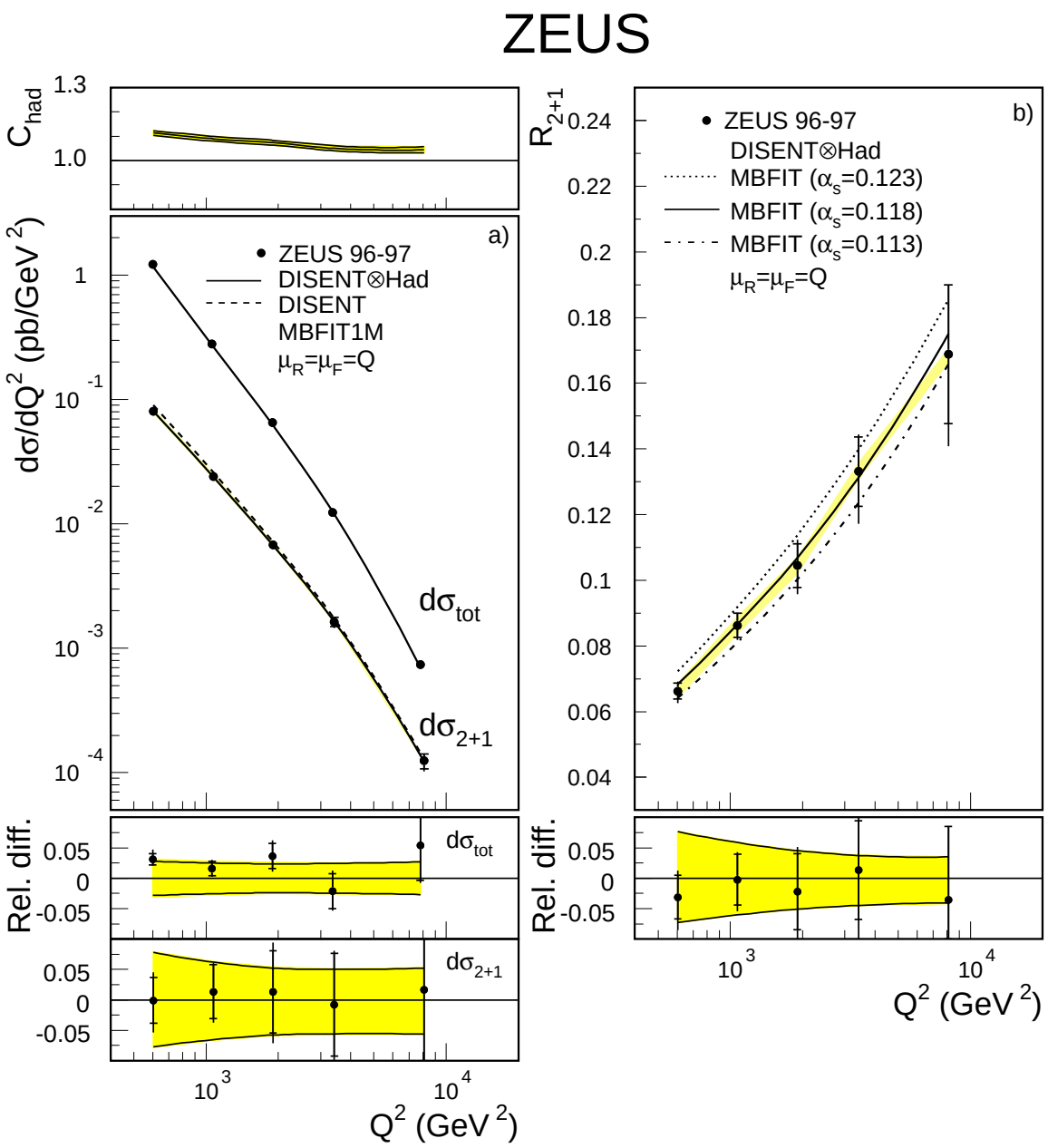

Figure 3: a) The measured inclusive ($d\sigma_{\rm tot}/dQ^2$) and dijet ($d\sigma_{2+1}/dQ^2$) differential cross sections in NC DIS as a function of Q^2. The hadronisation correction ($C_{\rm had}$), shown above the figure, refers to the dijet cross section. b) The dijet fraction, $R_{2+1}(Q^2)$, in NC DIS as a function of Q^2. The light shaded band displays the uncertainty due to the absolute energy scale of the jets. For comparison, the QCD predictions using MBFIT proton PDFs determined assuming $\alpha_s(M_Z) = 0.113$ and 0.123 [26] are also shown. The bands showing the theoretical uncertainty on the cross sections and dijet fraction do not include the uncertainty associated with $\alpha_s(M_Z)$. Other details are as described in the caption to Fig. 1.

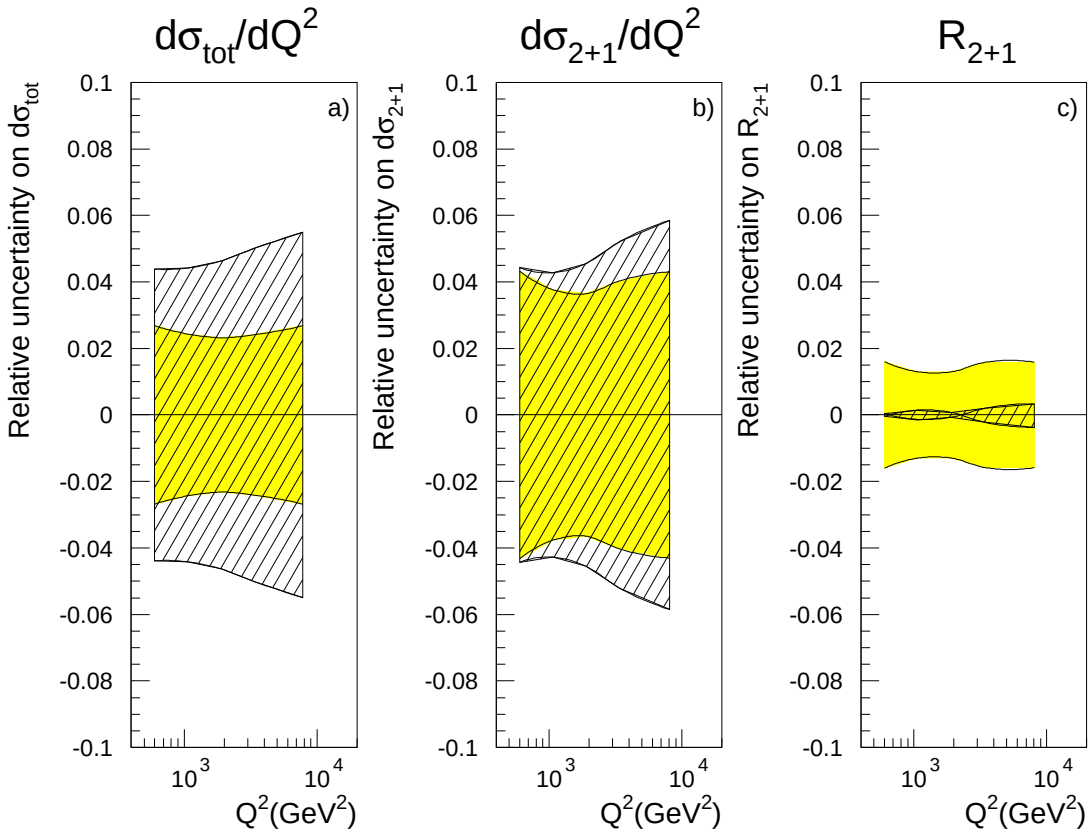

Figure 4: The relative uncertainty on a) the inclusive, b) dijet differential cross sections and c) the dijet fraction, due to the statistical and systematic experimental uncertainties of each data set used in the determination of the MBFIT PDFs. The shaded (hatched) bands indicate the uncertainties obtained (not) taking into account the correlations among the PDFs parameters.

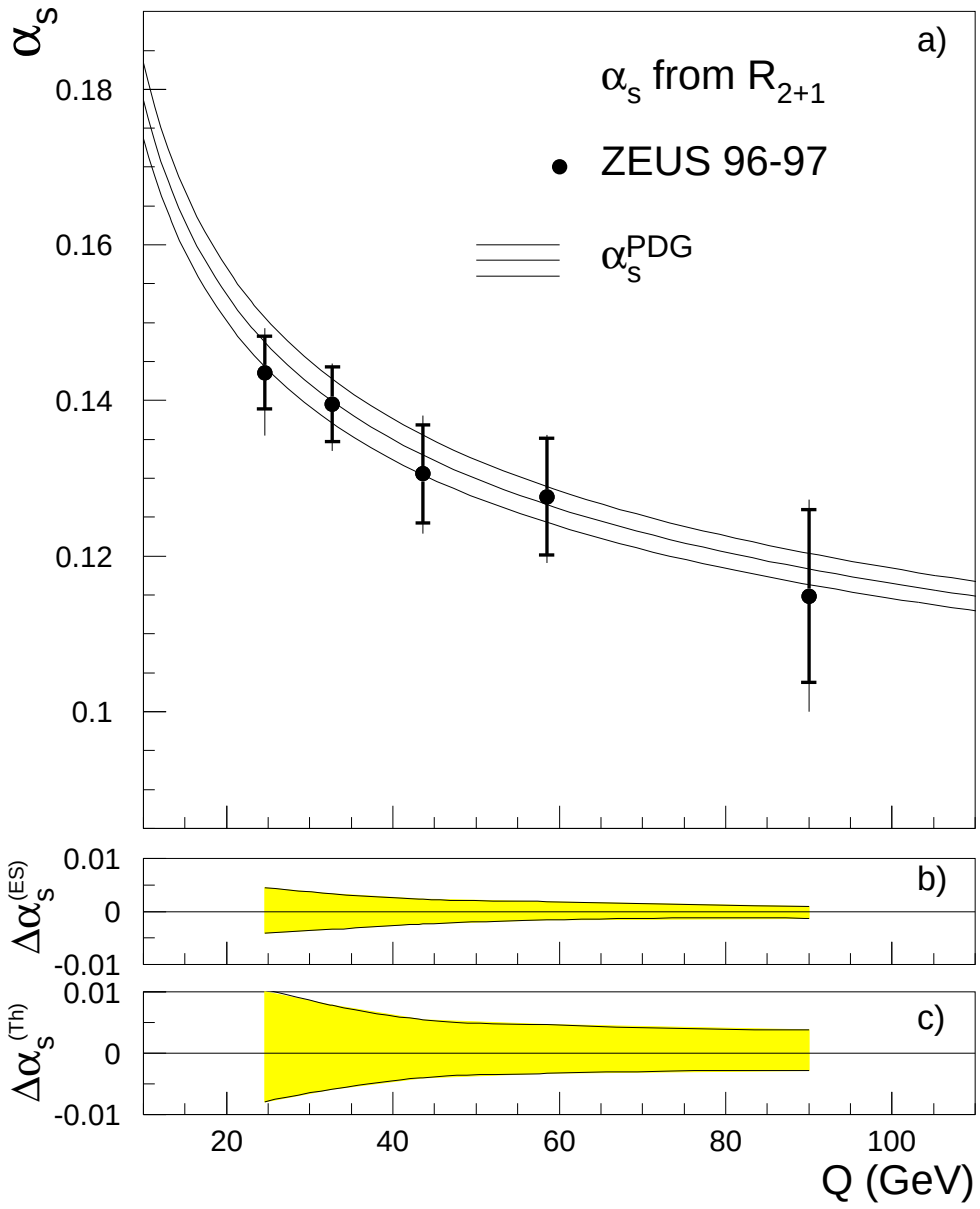

Figure 5: a) The $\alpha_s(Q)$ values determined from the QCD fit of the measured dijet fraction, $R_{2+1}(Q^2)$, as a function of Q. The inner error bars represent the statistical errors of the data. The outer error bars show the statistical errors and systematic uncertainties − except those associated with the uncertainty in the absolute energy scale of the jets − added in quadrature. The three curves indicate the renormalisation group predictions obtained from the PDG $\alpha_s(M_Z)$ value and its associated uncertainty. b) The uncertainty on α_s due to the absolute energy scale of the jets, $\Delta\alpha_s^{ES}$. c) The total theoretical uncertainty associated with the determination of α_s, $\Delta\alpha_s^{\rm Th}$.